# NAVAL POSTGRADUATE SCHOOL
# MONTEREY, CALIFORNIA

# THESIS

## DESIGN AND ANALYSIS OF A GAS TURBINE TEST FACILITY AIR SYSTEM

by

David D. Phelps

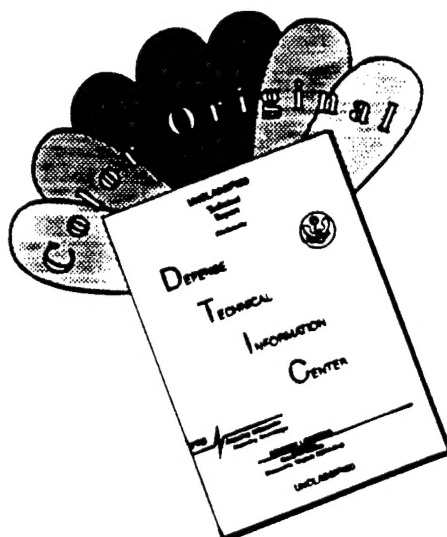December, 1995

Thesis Advisor:  Knox T. Millsaps, Jr.

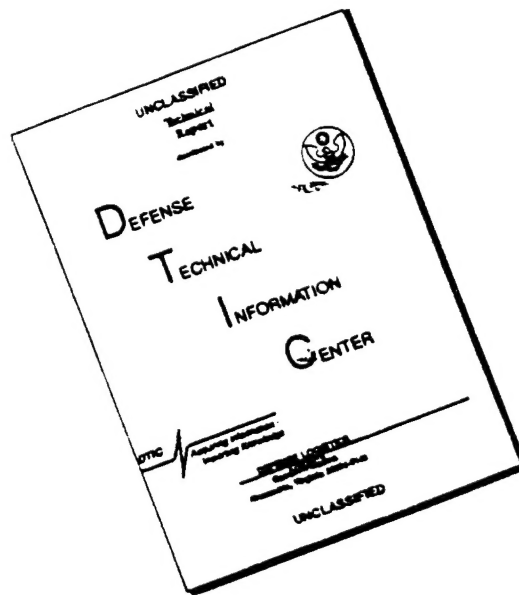**Approved for public release; distribution is unlimited.**

# 19960327 065

# DISCLAIMER NOTICE

THIS DOCUMENT IS BEST QUALITY AVAILABLE. THE COPY FURNISHED TO DTIC CONTAINED A SIGNIFICANT NUMBER OF COLOR PAGES WHICH DO NOT REPRODUCE LEGIBLY ON BLACK AND WHITE MICROFICHE.

# DISCLAIMER NOTICE

THIS DOCUMENT IS BEST QUALITY AVAILABLE. THE COPY FURNISHED TO DTIC CONTAINED A SIGNIFICANT NUMBER OF PAGES WHICH DO NOT REPRODUCE LEGIBLY.

# REPORT DOCUMENTATION PAGE

Form Approved OMB No. 0704-0188

| 1. AGENCY USE ONLY *(Leave blank)* | 2. REPORT DATE December 1995 | 3. REPORT TYPE AND DATES COVERED Master's Thesis |
|---|---|---|

| 4. TITLE AND SUBTITLE DESIGN AND ANALYSIS OF A GAS TURBINE TEST FACILITY AIR SYSTEM | 5. FUNDING NUMBERS |
|---|---|
| 6. AUTHOR(S) David D. Phelps | |

| 7. PERFORMING ORGANIZATION NAME(S) AND ADDRESS(ES) Naval Postgraduate School Monterey CA 93943-5000 | 8. PERFORMING ORGANIZATION REPORT NUMBER |
|---|---|

| 9. SPONSORING/MONITORING AGENCY NAME(S) AND ADDRESS(ES) | 10. SPONSORING/MONITORING AGENCY REPORT NUMBER |
|---|---|

11. SUPPLEMENTARY NOTES The views expressed in this thesis are those of the author and do not reflect the official policy or position of the Department of Defense or the U.S. Government.

| 12a. DISTRIBUTION/AVAILABILITY STATEMENT Approved for public release; distribution is unlimited. | 12b. DISTRIBUTION CODE |
|---|---|

13. ABSTRACT *(maximum 200 words)*

A gas turbine test facility air system has been designed to meet specified design objectives. An analytical evaluation was performed on the air system design to verify that these design objectives were achieved. A key element of the air system is an exhaust eductor which was included in the design to provide secondary cooling air flow through the engine test cell. Two analytical models were developed to evaluate exhaust eductor performance. A one-dimensional, incompressible eductor model was developed that predicts the basic eductor performance parameters including the amount of secondary air flow drawn through the engine test cell for varying eductor configurations. This model also predicts overall air system performance parameters. An eductor computational fluid dynamics analytical model was developed that provides a more detailed analysis of the flow in the eductor.

| 14. SUBJECT TERMS Eductor, Ejector, Computational Fluid Dynamics | 15. NUMBER OF PAGES 66 |
|---|---|
| | 16. PRICE CODE |

| 17. SECURITY CLASSIFICATION OF REPORT Unclassified | 18. SECURITY CLASSIFICATION OF THIS PAGE Unclassified | 19. SECURITY CLASSIFICATION OF ABSTRACT Unclassified | 20. LIMITATION OF ABSTRACT UL |
|---|---|---|---|

NSN 7540-01-280-5500

Standard Form 298 (Rev. 2-89)
Prescribed by ANSI Std. 239-18 298-102

# DESIGN AND ANALYSIS OF A GAS TURBINE TEST FACILITY AIR SYSTEM

David D. Phelps
Lieutenant, United States Navy
B.S., University of Tennessee, 1984

Submitted in partial fulfillment
of the requirements for the degree of

## MASTER OF SCIENCE IN MECHANICAL ENGINEERING

from the
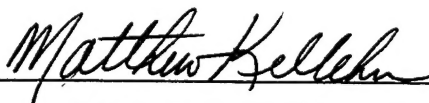
## NAVAL POSTGRADUATE SCHOOL
### December 1995

Author: _____

David D. Phelps

Approved by: _____

Knox T. Millsaps, Jr., Thesis Advisor

_____

Matthew D. Kelleher, Chairman,
Department of Mechanical Engineering

iii

# ABSTRACT

A gas turbine test facility air system has been designed to meet specified design objectives. An analytical evaluation was performed on the air system design to verify that these design objectives were achieved. A key element of the air system is an exhaust eductor which was included in the design to provide secondary cooling air flow through the engine test cell. Two analytical models were developed to evaluate exhaust eductor performance. A one-dimensional, incompressible eductor model was developed that predicts the basic eductor performance parameters including the amount of secondary air flow drawn through the engine test cell for varying eductor configurations. An eductor computational fluid dynamics analytical model was developed that provides a more detailed analysis of the flow in the eductor.

v

# TABLE OF CONTENTS

# LIST OF SYMBOLS

| **SYMBOLS** | **DEFINITION (units)** |
|---|---|
| a | speed of sound (ft/sec) |
| A | area ($ft^2$) |
| $C_p$ | constant pressure specific heat (ft lb/lbm R) |
| $C_v$ | constant volume specific heat (ft lb/lbm R) |
| e | total energy (ft lb/lbm) |
| $g_c$ | Newton constant = 32.174 ft lbm/lbf $s^2$ |
| h | height (ft) |
| P | pressure (lb/$ft^2$) |
| T | temperature (R) |
| w | mass flow rate (lbm/sec) |
| $\rho$ | density (lbm/$ft^3$) |
| $\xi$ | pressure loss coefficient |
| $\lambda$ | ratio of specific heats |
| $\upsilon$ | kinematic viscosity ($ft^2$/sec) |
| u | velocity in CFD computational domain x direction |
| v | velocity in CFD computational domain y direction |
| w | velocity in CFD computational domain z direction |

| **SUBSCRIPTS** | **DEFINITION** |
|---|---|
| atm | denotes ambient conditions |
| cell | denotes conditions in engine cell |
| b | denotes engine exhaust static conditions |
| c | denotes conditions at compressor inlet |
| o | denotes engine exhaust stagnation conditions |
| 1 | denotes conditions at exhaust nozzle outlet |

| | |
|---|---|
| 2 | denotes secondary flow conditions at eductor inlet |
| 3 | denotes eductor outlet conditions |
| e | denotes conditions at exhaust duct outlet |
| inf | denotes free stream conditions |

| **SUPERSCRIPTS** | **DEFINITION** |
|---|---|
| * | denotes CFD free stream normalized parameter |
| - | denotes CFD free stream normalized vector |

# I. INTRODUCTION

A gas turbine engine test cell is being constructed as part of the Mechanical Engineering Department Marine Propulsion Laboratory at the Naval Postgraduate School. The gas turbine test facility, which is intended for both student laboratory instruction and thesis research, consists of an Allison model 250-C18 gas turbine helicopter engine, a Superflow 901-SF waterbrake dynamometer test system, and the engine and dynamometer auxiliary support systems.

Among the gas turbine engine auxiliary support systems is the air system which must meet specific design objectives to facilitate proper operation of the engine and test cell. Specifically, the air system must:

- Supply clean and uniform primary air flow to the engine compressor at the required rate.
- Provide the capability to observe and measure the compressor inlet flow profile.
- Provide secondary air flow through the test cell for the purpose of test cell cooling.
- Maintain the compressor inlet pressure depression and engine back pressure below levels which would adversely effect engine performance.
- Provide engine noise attenuation capability.
- Provide air system safety shut-down capability in the event of emergency.
- Provide system performance measurement capabilities including engine air flow, cell pressure and temperature, compressor inlet pressure and flow uniformity, and engine exhaust pressure and temperature.

The purpose of this thesis project is to design an air system which fulfills the above requirements and to verify that these design objectives are achieved through analytical evaluation where possible. Individual components were designed or selected to perform specific functions while minimizing flow losses. These flow losses were estimated using one-dimensional Bernoulli's equations with pressure loss coefficients. The pressure loss coefficients were obtained either from standard hydraulics handbooks or from component manufacturers. Certain individual components were also selected based on recommendations from various sources including the engine manufacturer and gas turbine cell designers.

Two important features of the air system design are an inlet plenum and an exhaust eductor. The function of the inlet plenum is to provide uniform air flow to the engine compressor. It houses a series of perforated plates, fine-mesh screens, and a honeycomb screen selected to achieve this goal. Since the compressor inlet profile cannot be predicted analytically, the inlet plenum is designed to allow visualization

and measurement of the compressor inlet flow profile so that greater flow uniformity can be achieved through iterative experimentation.

An exhaust eductor is included in the design to provide secondary air flow through the test cell for cooling purposes. Two analytical models were developed to analyze the basic eductor design. A one-dimensional, incompressible model was developed to evaluate the eductor performance. This model predicts the amount of secondary air flow drawn through the cell for various eductor nozzle sizes at full engine power operation. It also predicts various air system performance parameters for each of these eductor configurations including cell pressure, compressor inlet pressure, eductor exhaust pressure and temperature, and engine back pressure. A preliminary computational fluid dynamics (CFD) model was also developed to provide a more precise analysis of the flow in the eductor.

Chapter II provides background information on eductors. The fundamentals of eductor operation and the basic design factors which determine eductor performance are described. Previous analytical and experimental research aimed at predicting and evaluating eductor performance is also cited.

Chapter III provides a complete description of the air system designed for the gas turbine test cell. Air system design considerations and methodologies are also described.

The one-dimensional, incompressible eductor model developed to predict eductor and overall air system performance is described in Chapter IV. The MATLAB code written based on this model is also described along with the results.

Chapter V describes the CFD model of the exhaust eductor, including a general description of the CFD algorithm employed. The physical grid, input files and results are also presented. Velocity profiles obtained from the CFD model are then compared to velocity profiles obtained experimentally for an eductor of similar geometry.

Conclusions and recommendations are included in Chapter VI.

2

# II. BACKGROUND ON EXHAUST EDUCTORS

## A. EDUCTOR OPERATION

The basic operation of an exhaust eductor is described by reference to Figure (1). In general, the eductor consists of an engine exhaust nozzle which is mounted in the region of a duct or shroud. The high temperature, high velocity exhaust primary flow ($w_p$) is expelled from the nozzle at a velocity $V_1$ into the duct. Lower temperature ambient air from the cell is entrained into the jet due to viscous mixing at the periphery. The entrained air is replaced by air further upstream in the cell and consequently a secondary flow ($w_s$) at a velocity of $V_2$ is developed as indicated in Figure (1). The secondary flow carries heat away from the engine cell as it is drawn into the eductor and mixes with the primary flow. The mixing of the two flow streams in the eductor results in the reduction of the exhaust gas temperature. The amount of secondary air drawn from the cell and the degree of mixing that takes place in the eductor determine the amount of heat that is carried away from the cell and the amount of exhaust gas temperature reduction achieved. These quantities are determined by several factors including the total energy of the primary flow, engine cell pressure, the total pressure loss downstream of the eductor, and eductor geometry.

Discharge of the high-temperature, high-velocity, jet-type flow into the eductor initiates a highly-turbulent mixing process between the two streams. The lateral transfer of momentum and energy during this mixing process causes both the temperature and velocity profiles to flatten-out and widen in the downstream direction. This effect is illustrated in Figure (2) from Reference (3), which shows the development of velocity profiles in a free jet. Turbulent mixing between the primary jet and the entrained secondary flow results in the flow becoming gradually more uniform in the downstream direction. Flow in an eductor is similar to that of a free jet in that the non-uniformities in temperature and velocity gradually decrease downstream of mixing duct entrance. Eventually plug-type profiles will develop at some finite point downstream in the mixing duct, assuming the duct is of sufficient length.

## B. EDUCTOR PERFORMANCE

Eductor performance is generally quantified by the amount of secondary air flow drawn for a given primary flow and by the degree of mixing achieved at the eductor outlet. Eductor geometry strongly influences these performance parameters. Reference (4) describes a one-dimensional, compressible method of analysis developed to predict the performance of a constant-area gas eductor. Referring to Figure (1), constant area eductors are superior to constant pressure eductors because they can pump the secondary fluid

to an eductor exit pressure $P_3$ which is higher than $P_{cell}$. Thus constant area eductors act as pumps whereas constant pressure eductors can only serve as blowers or fans. Experimental data were collected in Reference (4) for the purpose of testing the validity of the method of solution. These results also provide insight into eductor design considerations.

The experimental data were collected in Reference (4) on a cylindrical eductor and conclusions drawn can be summarized as follows:
- Higher secondary to primary flow ratios are achieved by constant area eductors than constant pressure eductors.
- The secondary to primary flow ratio increases as the primary nozzle is moved upstream from the eductor throat to a distance equal to 1/2 the eductor throat diameter. The maximum flow ratio is achieved at this point and decreases as the primary nozzle is moved further upstream. It should be noted that the rate of increasing flow ratio is very small and that the flow ratio attained with placement of the primary nozzle in the throat was only one to three percent less than the maximum. Furthermore it was found that the best position for primary nozzle placement was independent of the pressure ratio $P_0/P_{cell}$ and the eductor area ratio $A_e/A_n$.
- The secondary to primary flow ratio increases with increasing eductor area ratio $A_e/A_n$, independent of the pressure ratio $P_0/P_{cell}$. This parameter has the most significant effect on eductor performance.
- The secondary to primary flow ratio increases with increasing eductor length to eductor diameter ratio to a maximum value and then decreases. The best eductor length is slightly greater than seven eductor diameters based on the experimental results from reference (2).
- The degree of mixing achieved increases with increasing eductor length.

Reference (5) describes experimental results obtained for multiple nozzle eductors, and concluded that the eductor to primary nozzle area ratio had the most effect on eductor performance. It also found that moving the primary nozzle upstream from the eductor throat led to a slight increase in eductor performance, although the primary nozzles were moved only a small amount upstream during these experiments. These results fundamentally reaffirm those obtained in Reference (4).
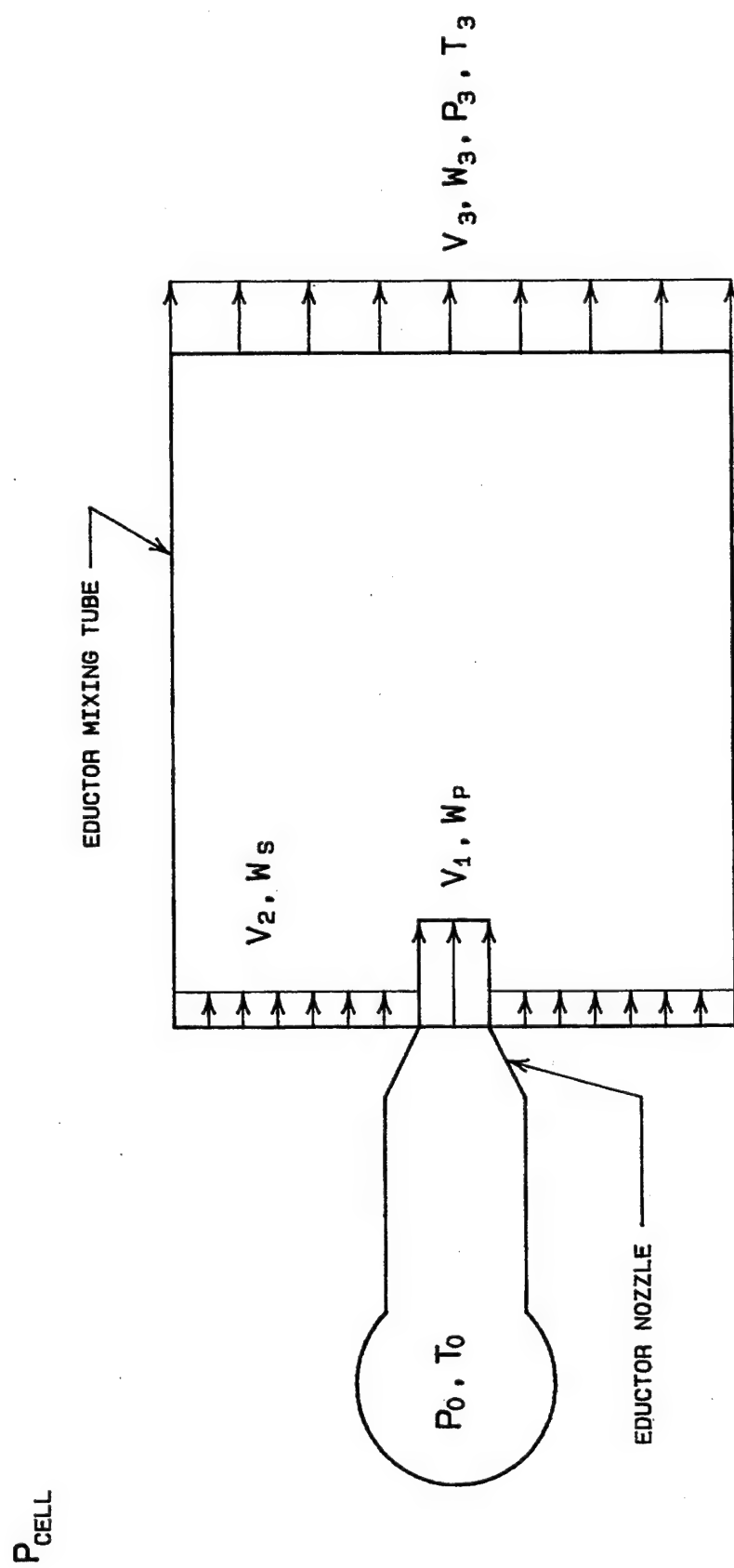
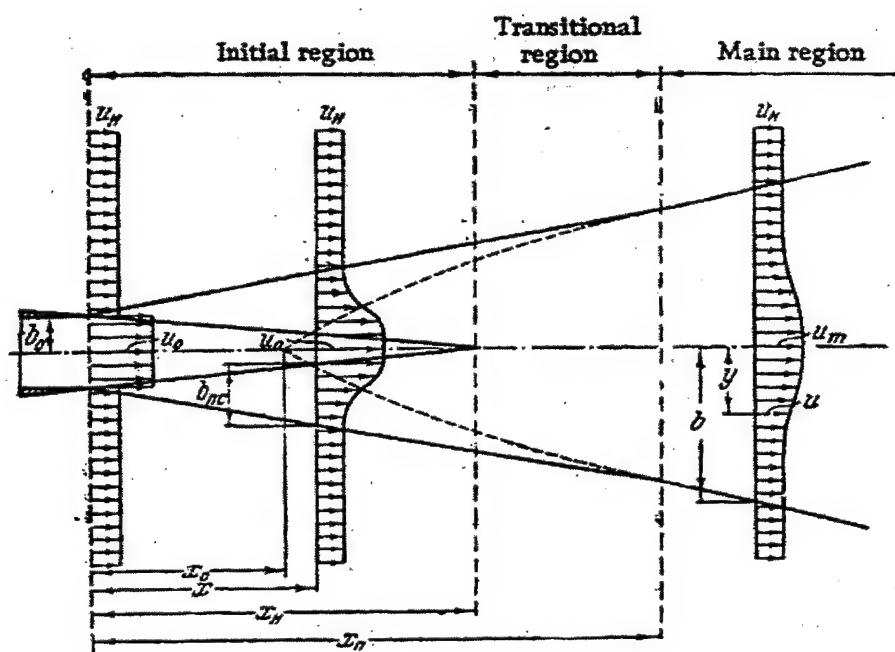Figure 1. Eductor Operation Schematic.

5

Figure 2. Free Jet Entrainment and Mixing, (from ref(3)).

# III. GAS TURBINE TEST CELL AIR SYSTEM DESIGN

The air system was designed to support proper operation of the engine at full power conditions. The engine installed in the test cell is an Allison model 250-C18 turboshaft helicopter engine. At 100 percent compressor speed (51,120 rpm) and 100 percent power turbine speed (35,000 rpm) the design output power is 317 horsepower. Engine air flow under these conditions is approximately 3.15 lbm/sec or 2500 SCFM and exhaust is discharged at approximately 1060F.

## A. AIR SYSTEM DESIGN REQUIREMENTS

The first step in developing the system design was to determine the system requirements as specifically as possible. System requirements were determined either from the engine operating manual (Reference 6) or through consultation with various sources including the engine manufacturer, gas turbine cell manufacturers, and the test cell instrumentation manufacturer. The specific air system design requirements are:

1. The air system must provide air flow to the engine at a rate of 3.15 lbm/sec or 2500 SCFM at engine full power operating conditions. Furthermore, the air flow supplied to the engine compressor must be clean and uniform. The system must provide the capability to observe and measure the uniformity of the flow profile at the compressor inlet. Cleanliness requirements specified by the engine manufacturer were that the air filter must filter out particles sizes in excess of one micron with 95 percent efficiency.
2. Secondary air flow through the test cell is required in order to cool the cell. Based on the engine rating and test cell size the secondary air flow requirement was determined to be approximately one room change out per minute or 3000 SCFM.
3. The air system must provide the capability to attenuate engine noise within the frequency range of 20 Hz to 20 kHz with 20 dB attenuation to the engine control room.
4. Safety shutdown devices capable of securing air flow into the test cell in cases of emergency must be included in the air system design.
5. System performance measurement capability must be provided. Specifically, the system must provide the capability to measure cell pressure and temperature, compressor inlet pressure and temperature, engine primary air flow rate, and engine exhaust pressure and temperature.
6. Compressor inlet pressure depression must be maintained below a level which would adversely effect engine performance. The maximum compressor inlet depression allowable was determined to be 6 in $H_2O$ based on consultation with the engine manufacturer.

7

7. Engine back pressure must also be maintained below a level which would adversely effect engine performance.

The requirements to minimize compressor inlet pressure depression and engine back pressure required evaluation of the pressure loss across each system component. Pressure loss calculations were performed using Equation (1). Values for the pressure loss coefficients ($\xi$) for individual components were determined either from hydraulics handbooks, References (1) and (2), or from information supplied by the component manufacturer.

$$P_L = \frac{\xi \rho V^2}{2g_c} \tag{1}$$

where:

$P_L$ = pressure loss across component (lb/ft$^2$)

$\xi$ = pressure loss coefficient of component

$\rho$ = density of the airflow (lbm/ft$^3$)

$V$ = velocity of the air flow (ft/sec)

The overall test cell air system is shown in dimensioned plan and elevation views in Figure (3) and Figure (4) respectively. The system consists of the gas turbine engine and four subsystems, the inlet ducting, the inlet plenum, the engine exhaust piping and eductor, and the exhaust ducting. Each subsystem was designed to perform specific functions in order to fulfill the overall air system design requirements. The remainder of this chapter is devoted to describing each subsystem.

## B. AIR INLET DUCTING

Plan and elevation views of the air inlet ducting are shown in Figure (3) and Figure (4) respectively. The stainless steel inlet ducting, which was sized based on pressure loss calculations, consists of a 10 foot horizontal run with a 71 inch by 36 inch rectangular cross section. The air is turned 90 degrees and enters the space through a 48 inch by 48 inch square section of ducting which is 18 inches in length.

Referring to Figure (3), air enters the inlet duct through a set of inlet louvers and a 1/2 inch square grid 1/16 inch gauge inlet screen installed to prevent large particles of airborne debris from being pulled into the cell. Just inside the screen is a set of fire control shutters designed to close in the event of a fire in the test cell. The shutters are spring-loaded open and are released by the action of temperature detectors located in the cell thereby eliminating air supply to the cell. After the fire control shutters the air flows through a row of seven silencers which were designed to meet the engine noise attenuation requirements.

The silencers have a 7 inch by 36 inch rectangular cross section and are 30 inches in length. The leading edges of the silencers are rounded for the purpose of reducing flow losses.

Air is then turned downwards into the cell through the 48 inch by 48 inch square duct. At the top of this duct the air passes through a set of four 24 inch by 24 inch air filters. The air filters provide air filtration of particles equal to or greater than one micron in size at 95 percent efficiency. The filters were selected based on air filter performance recommendations from the engine manufacturer. Figure (5) shows the pressure loss across clean filters as a function of flow rate for the model of filter selected. This information was provided by the filter manufacturer.

Adjustable shutters are installed at the bottom of the 24 inch by 24 inch square duct to guide airflow into the cell toward the engine. The shutters are linked to an electrical motor which holds the shutters open when energized against spring tension. The shutters close automatically under spring tension when power is secured to the motor thereby closing off air flow into the space in the event of an emergency.

## C. AIR INLET PLENUM

The air inlet plenum is shown in Figures (6a) and (6b). The inlet plenum is fabricated from 1/4 inch clear plexiglass and aluminum supports. Clear plexiglass was selected to facilitate observation of flow into the compressor. Two nine inch diameter turbine flow meters are mounted side by side on the front wall of the plenum and the engine compressor bell housing extends into the plenum through the back wall. The turbine flow meters are part of the dynamometer test system instrumentation and are rated at 1200 SCFM. The flow meters are wired in parallel to increase the measurement range to 2400 SCFM which is the maximum engine air flow rate. The front half of the plenum has a 36 inch by 36 inch cross section which decreases down to a 12 inch by 12 inch cross section at the back wall.

The exit diameter of the flow meters is eight inches which has a nozzling effect on the air flow resulting in jet type flow. The front half of the plenum houses a series of perforated plates and screens designed to modify the jet type flow profile into a more uniform flow profile. The last screen in the front half of the plenum is a honeycomb screen, which breaks up large scale flow structures like axial vortices. Honeycomb screens are often employed in wind tunnels for this purpose. The flow is then contracted down in the back half of the tunnel in order to reduce spatial non-uniformity in the flow at the compressor inlet.

As can be seen in Figure (7a) from Reference (2) the perforated plates exert an equalizing influence on the jet flow profile. The perforated plates create a resistance that causes the incoming flow to spread out over the surface of the plates and simultaneously cross through the orifices in the plates. The

9

degree of equalizing influence exerted on the flow is dependent on the geometrical properties of the plate, primarily the free area ratio and the plate thickness, and thus is a function of the flow resistance coefficient of the plate. As can be seen in Figure (7a) from Reference (2), increasing flow resistance causes a greater degree of spread across the surface of the plate resulting in a greater degree of equalizing influence. In thin wall grids however there is a certain limiting value of resistance coefficient which results in the velocity profile downstream of the plate becoming overturned.

This effect can be explained using Figure (7b) also from Reference (2). As the incoming flow spreads out over the surface of the plate the flow develops radial velocity components. In thin wall plates these radial components are retained to a greater degree after the flow passes through the orifices because the orifices are not deep enough to turn the flow back in the axial direction. This radial distortion of the velocity profile downstream of the plate increases with increasing resistance coefficient. With increases of loss coefficient up to a certain value the central portion of the jet can loose all of its axial velocity and can even become reversed by entrainment of the circumferential jets as can be seen in Figure (7b). Figure (7a) shows this effect starting to happen at a value of loss coefficient $\xi$ equal to 2.8. At this value of $\xi$ it can be seen that the axial velocity component of the center portion of the jet begins to decrease. At a value of $\xi$ equal to 1.2 a high degree of uniformity is developed in the profile developed without incurring the reversing effects in the center portion of the jet as described above. These profiles suggest that values of $\xi$ between 1.2 and 2.8 would have the desired equalizing effect that would begin to make the flow more uniform.

Greater flow uniformity can also be created through the use of fine-mesh screens. Screens are commonly found in wind tunnels for this purpose. Figure (8a) from Reference (7) illustrates the effect that a typical fine-mesh screen employed in wind tunnels has on a jet-type velocity profile. Figure (8b) from the same reference shows the relationship between pressure loss coefficient and velocity for various types of fine-mesh screens.

The inlet plenum as shown in Figures (6a) and (6b), is designed to break up the jet type flow and achieve greater flow uniformity in stages. Upon exiting the flow meters the flow first encounters a 1/8 inch thick perforated plate with one inch diameter holes. This is followed by a more restrictive 1/8 inch perforated plate with 1/2 inch diameter holes. The loss coefficients for these plates are 1.7 and 2.4 respectively. Greater uniformity is achieved as the flow passes through a series of two fine-mesh screens. The first screen is 18- mesh, 0.011 inch wire diameter, and the second screen is a more restrictive 20-mesh, 0.017 wire diameter. Downstream of the fine-mesh screens is a 1inch thick, 1/8 inch hexagonal cell, honeycomb screen, which removes the large scale flow structures as was previously stated. The back section

10

of the plenum contracts and guides the flow into the compressor bellmouth. The nine to one area contraction takes place over a length of 3 feet to facilitate the reduction of spatial non-uniformity in the flow.

The hinged and slotted construction of the plenum allows flexibility in screen and plate selection and placement. These features combined with the use of clear plexiglass provide the capability to monitor and modify the flow into the compressor. The compressor inlet flow profile can therefore be optimized through iterative experimentation.

## D. TEST CELL EXHAUST DUCTING

Plan and elevation views of the stainless steel exhaust ducting are shown in Figure (3) and Figure (4) respectively. The ducting is fabricated from 316 stainless steel due to the high temperature application and for its corrosion resistant properties. The entrance section of the exhaust ducting which is 42 inches in length with a 36 inch by 36 inch square cross section turns the flow ninety degrees into a 36 inch long, horizontal section of ducting with the same cross section. The ducting is then transitioned to a 36-inch diameter circular cross section by a 24 inch long transition piece which is followed by a 24 inch long section that exits the building.

The exterior section of the exhaust ducting is shown in Figure (9). This 3 foot diameter, stainless steel ducting consists of a ninety degree elbow followed by a 35 foot long vertical section that terminates 7 feet above the roof of the building. An inverted cone type weather cover is installed at the piping exit.

## E. ENGINE EXHAUST PIPING AND EDUCTOR

The engine exhaust piping is shown in Figures (10a) and (10b). Two 8 inch diameter, stainless steel exhaust pipes carry engine exhaust from the elliptical engine exhaust ports to a position just below the exhaust duct. Elliptical flanges on the exhaust elbows are mated to the exhaust port flanges and secured with a C-clamp. The C-clamps are manufactured by Bell Helicopter specifically for this purpose. The elbows transition the exhaust piping from a 5 inch by 7 inch elliptical cross section to an 8 inch diameter circular cross section. The overall length of each exhaust pipe is approximately 64 inches. The exhaust pipes terminate just below the exhaust ducting and are centered in the exhaust ducting .

As is shown in Figure (10b), the exhaust pipes are supported by rollers which are mounted on the engine/dynamometer frame. This support arrangement allows unconstrained exhaust pipe thermal expansion which reduces the axial stress transmitted to the exhaust port C-clamp connection.

11

The flanged eductor nozzles are mounted on the exhaust pipe flanges as shown in. A series of 6-inch, 3-inch, and 1-inch flanged spacers were fabricated to provide the capability of varying the separation between the eductor nozzle exit and exhaust ducting inlet. This separation can be varied from a maximum of 22 inches to a minimum of 0 which corresponds to the nozzle exit positioned in the throat of the exhaust duct.

The basic eductor configuration is shown in Figure (11). The two eductor nozzles are centered just below the entrance to the exhaust ducting. The exhaust ducting serves as the eductor mixing tube or shroud. Several different nozzle sizes ranging from 8 inches to 6 inches in exit diameter were fabricated for testing. These design features provide the capability of varying the eductor nozzle diameter and the nozzle to eductor separation in order to test various configurations. The optimum configuration is that configuration which provides the most secondary flow through the test cell without imposing excessive back-pressure on the engine.

An obvious potential problem with the basic eductor configuration is illustrated in Figure (11). The inlet section to the exhaust ducting, which is only 18 inches in length, is followed by a 90 degree bend. The concern is that the length of the straight section of inlet ducting is not sufficient to allow enough mixing to occur. This tends to result in increased losses in the 90 degree bend. Increasing the nozzle to ducting separation will result in an increased mixing length which may serve to mitigate this potential problem. Results from Reference (4) indicate that the optimum placement of the nozzles should be approximately 18 inches below the ducting inlet.
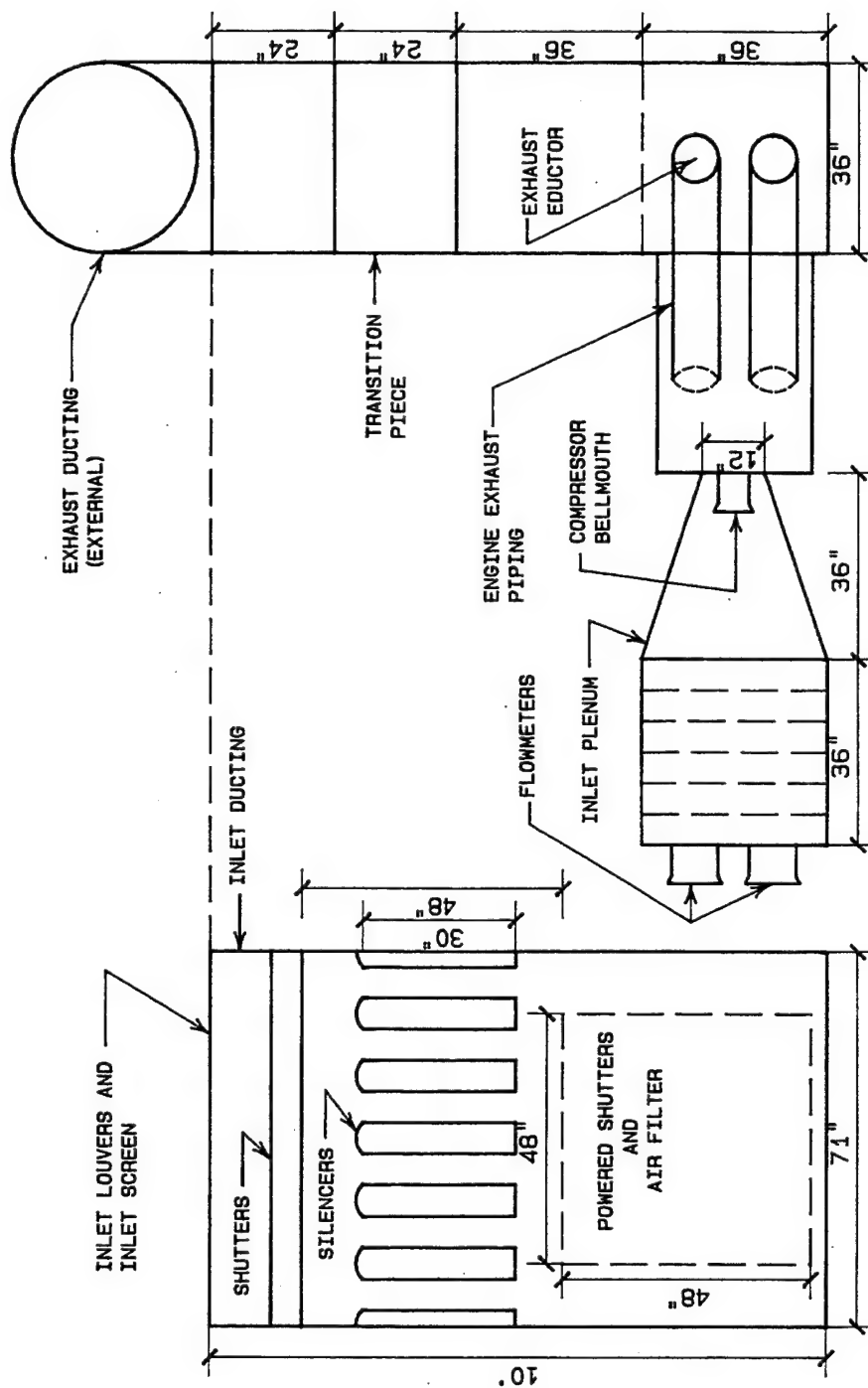
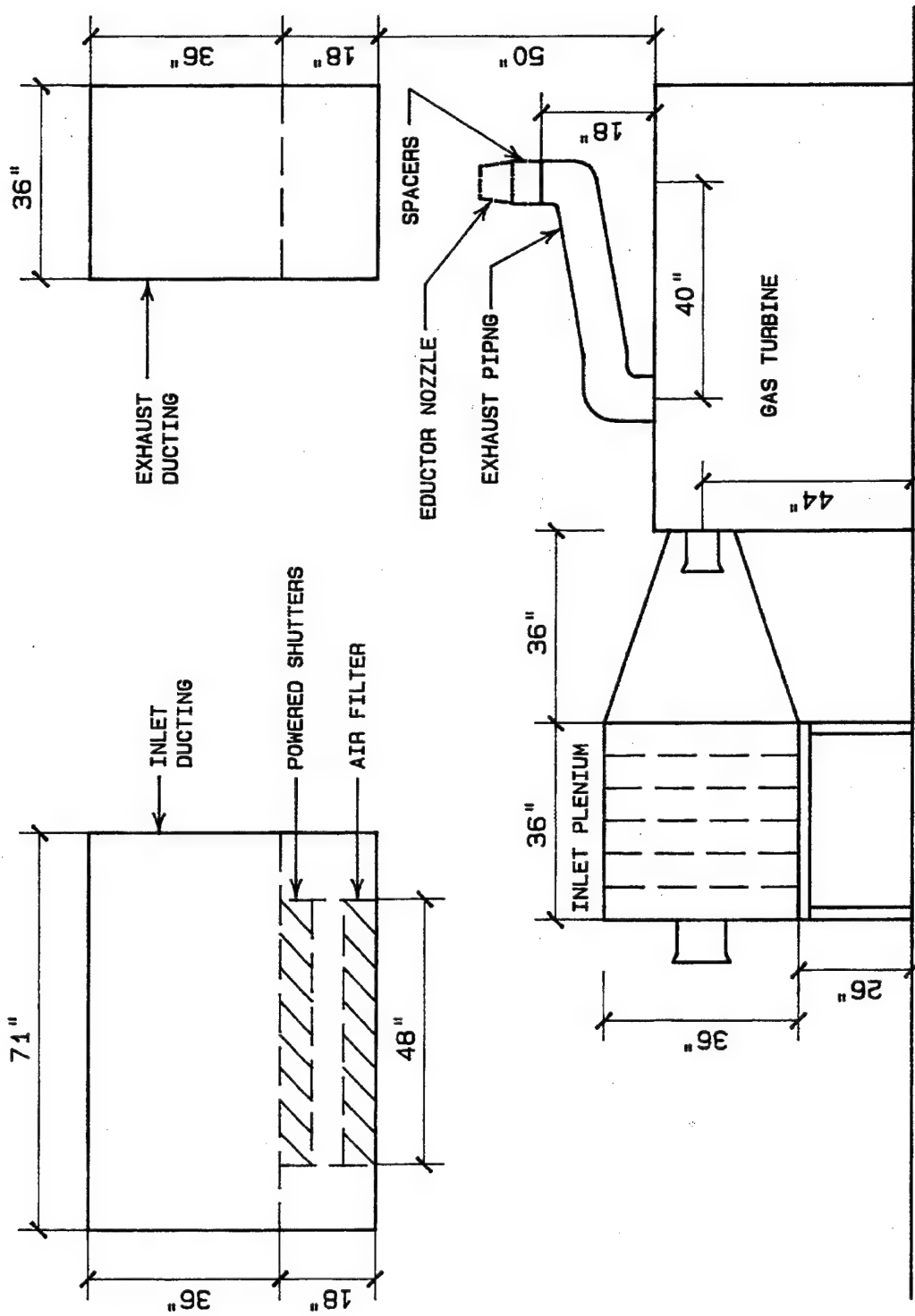Figure 3. Gas Turbine Test Cell Air System, Plan View.

13

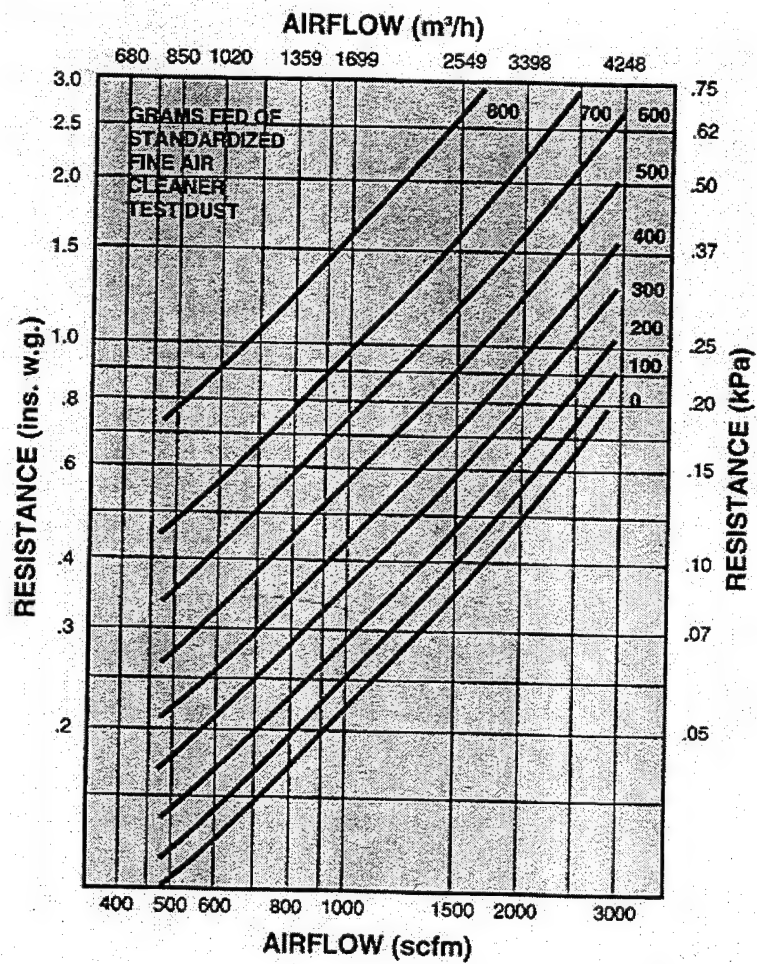Figure 4. Gas Turbine Test Cell Air System, Elevation View.

Figure 5. Inlet Air Filter Pressure Loss.

Figure 6b. Inlet Plenum, Side View.



Figure 6b. Inlet Plenum, Side View.

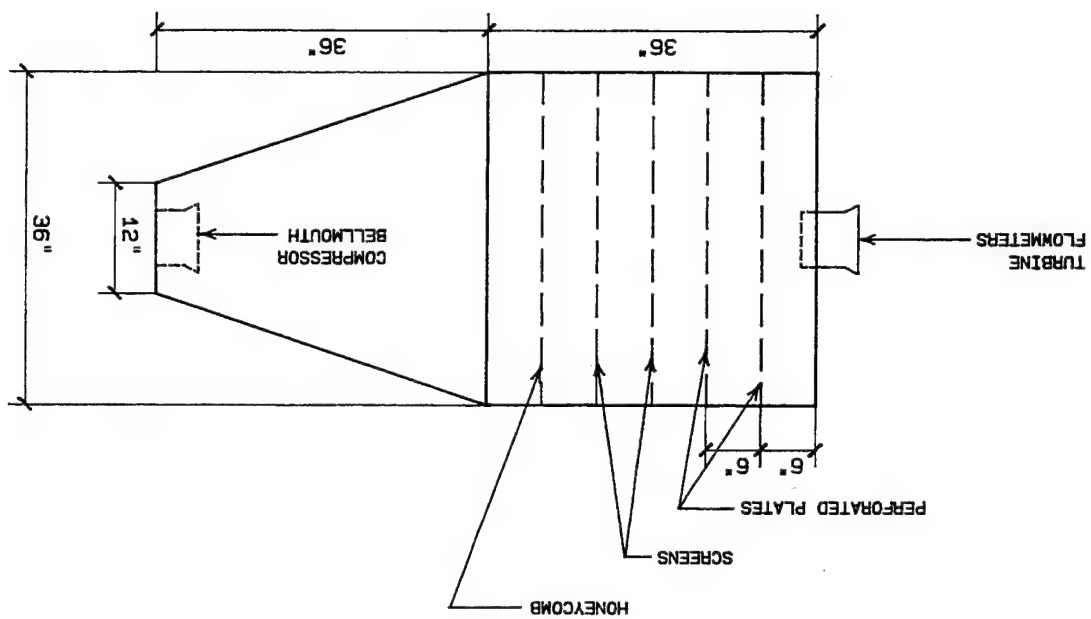Figure 6a. Inlet Plenum, Top View.



Figure 6a. Inlet Plenum, Top View.
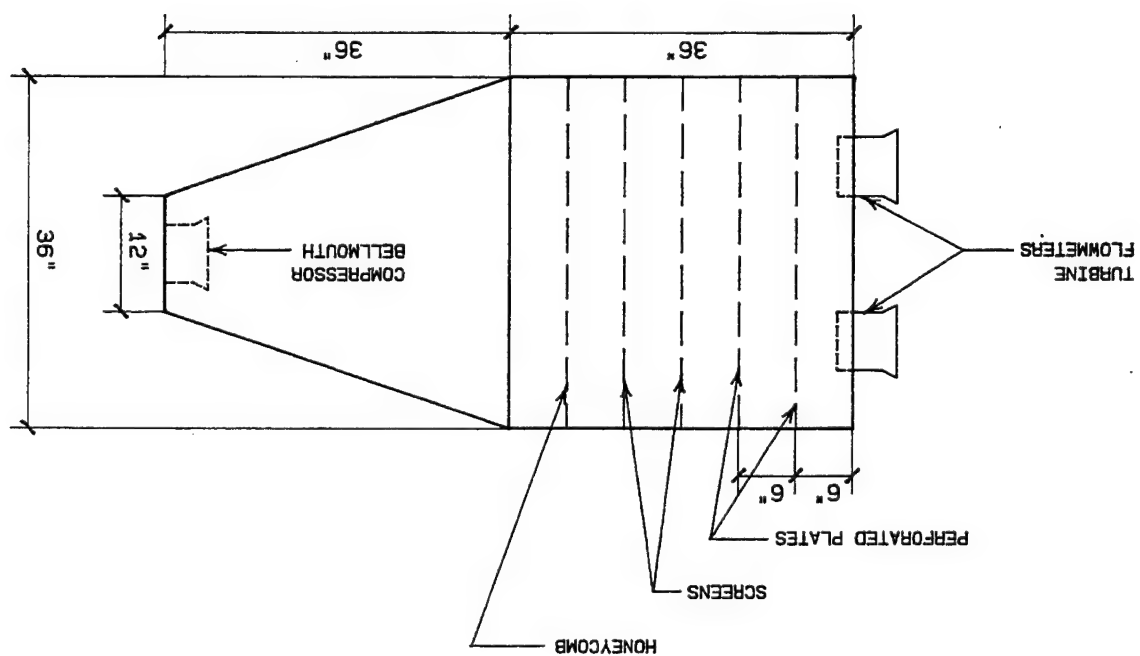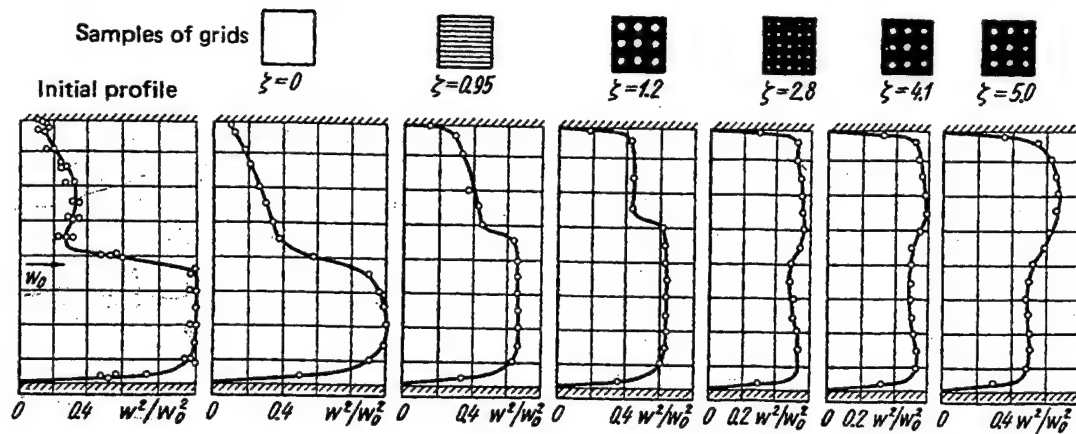
Figure 7a. Equalizing Effect of Perforated Plates on Jet Flow Profile, "from Ref (2)".
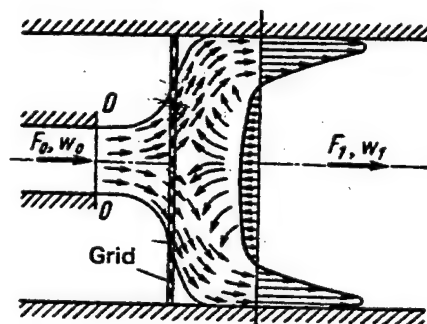


Figure 7b. Effect of Overly Restrictive Grid on Jet Profile, " from Ref (2)".

17

Figure 8a. Equalizing Effect of Fine-Mesh Screens on Jet Flow, "from Ref (7)".
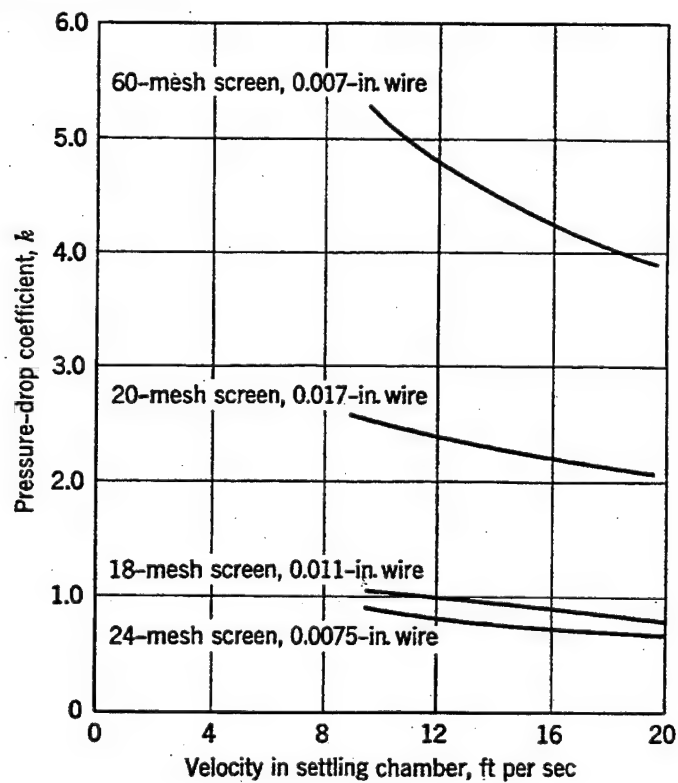


Figure 8b. Fine-mesh Screen Pressure Loss Coefficients, "from Ref (7)".

WEATHER COVER

3' DIAMETER

35'

Figure 9. External Exhaust Ducting.

Figure 10a. Engine Exhaust Piping, Top View.

Figure 10b. Engine Exhaust Piping, Side View.

21

Figure 11. Test Cell Eductor Configuration.

# IV. ONE-DIMENSIONAL, INCOMPRESSIBLE EDUCTOR MODEL

## A. INTRODUCTION

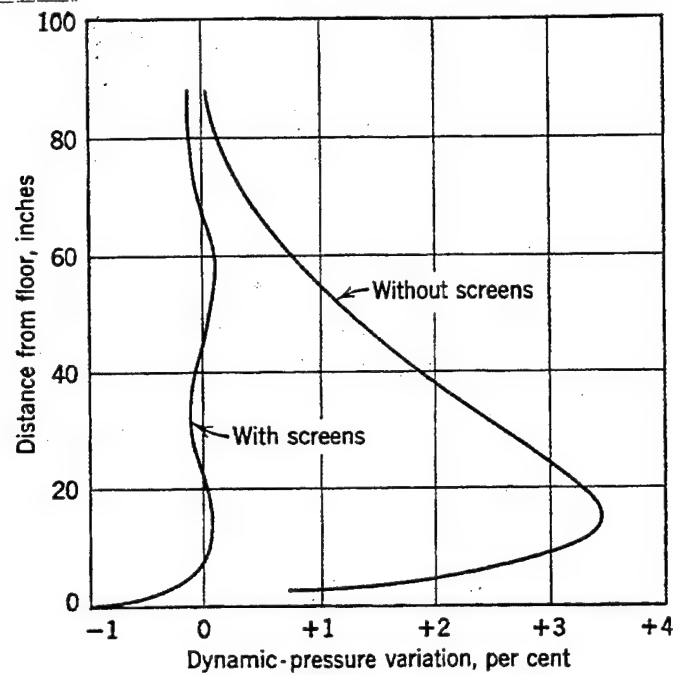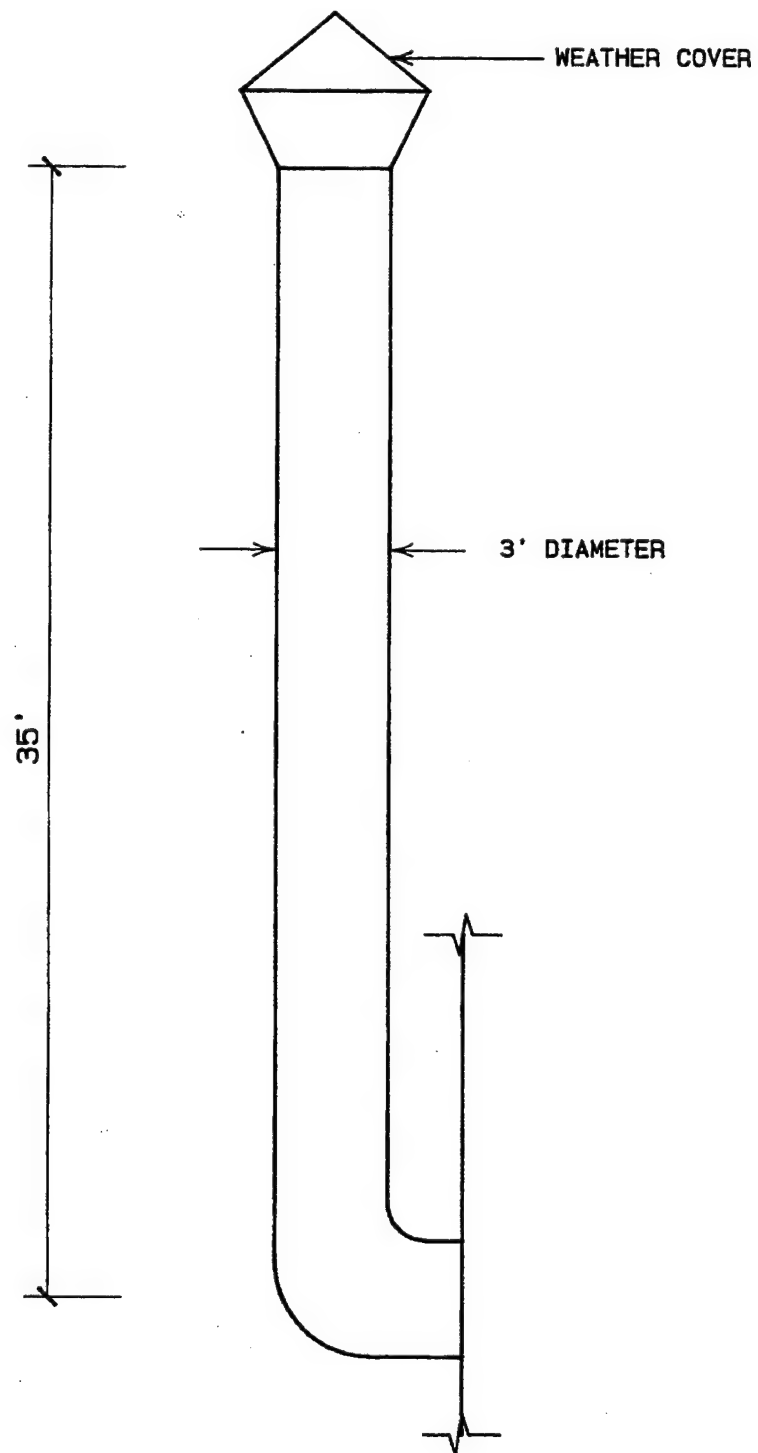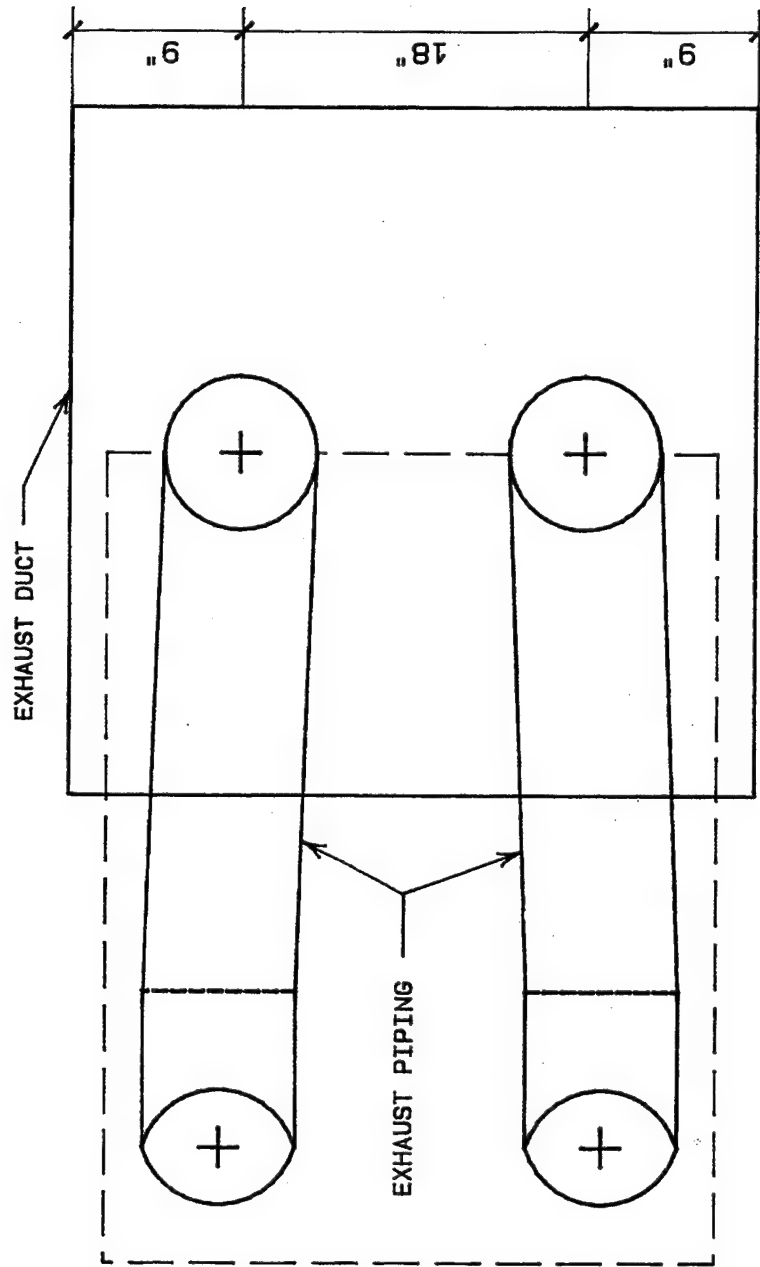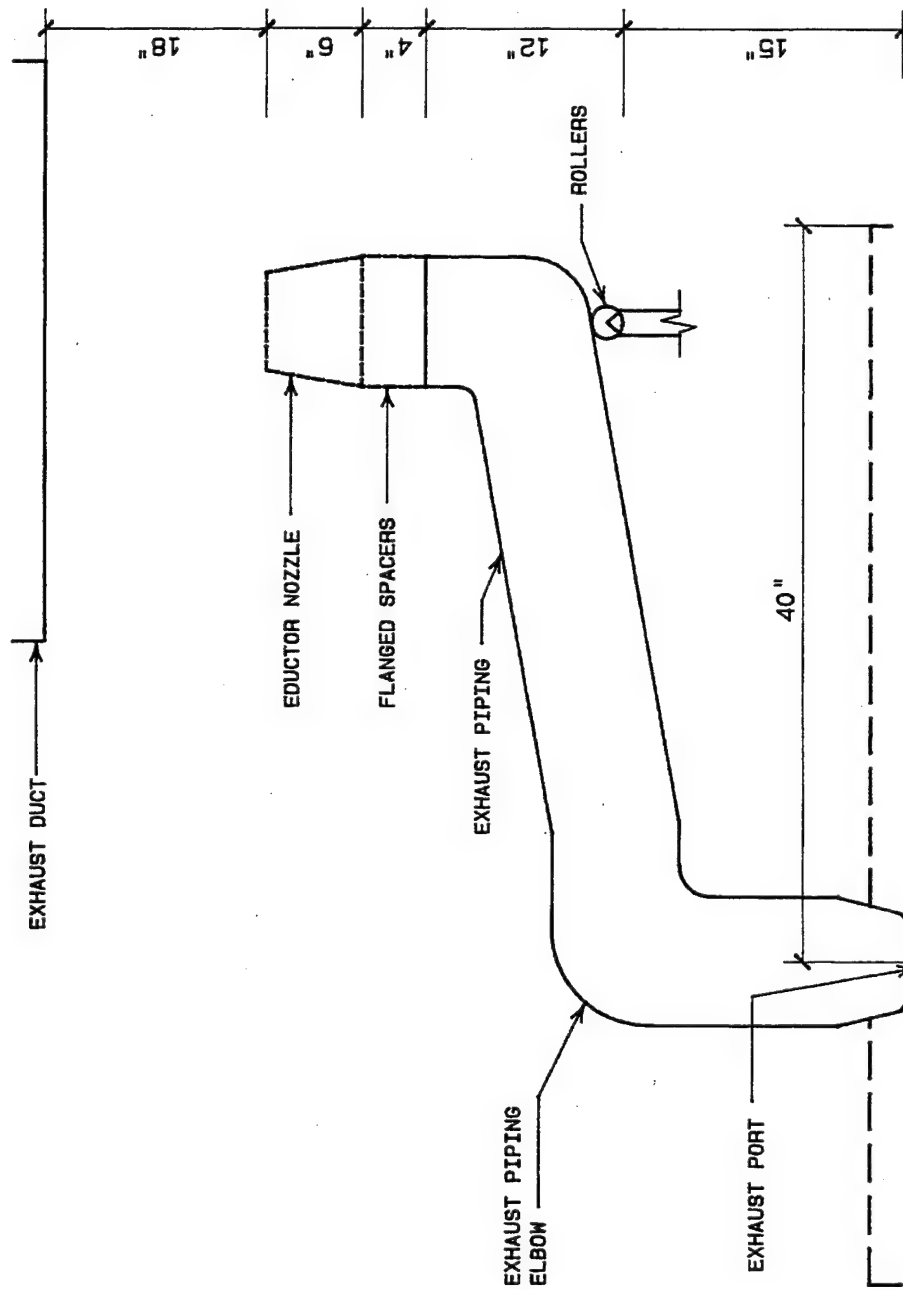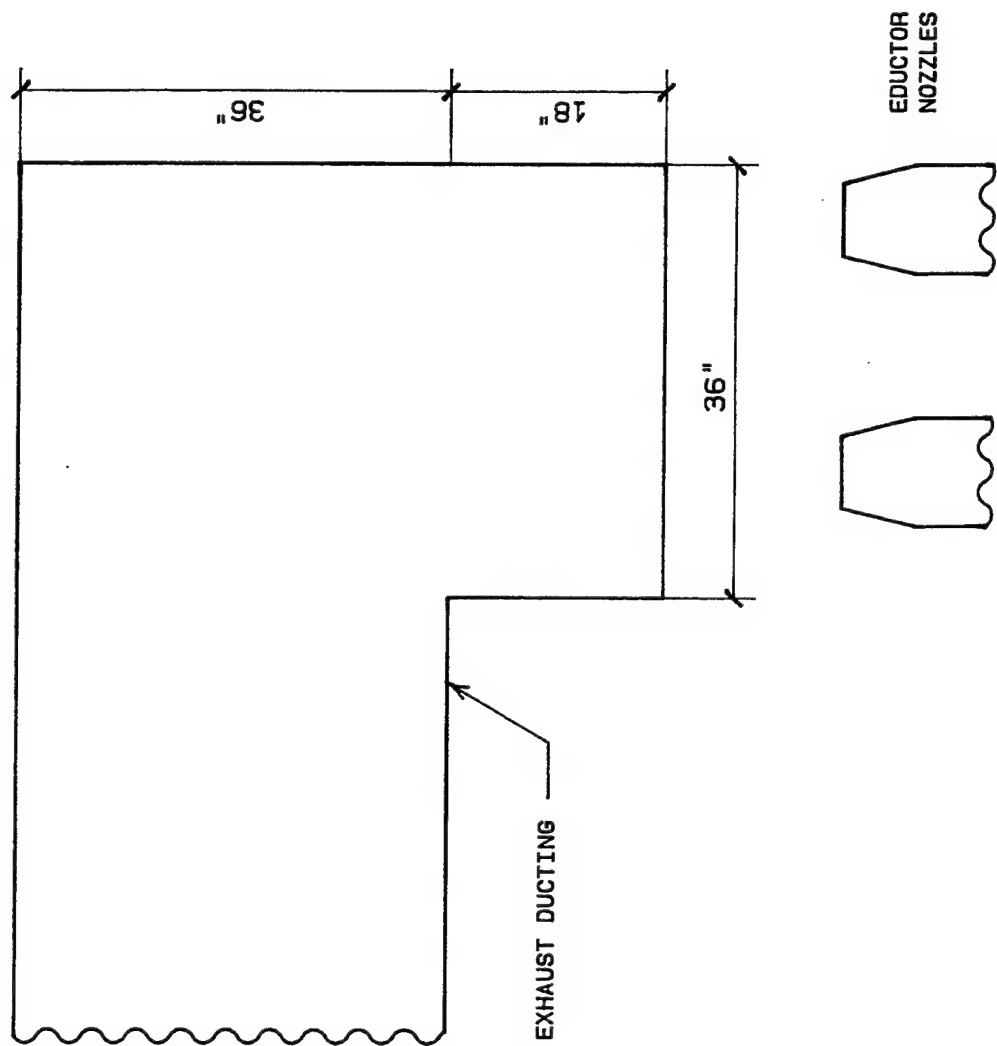The purpose of the eductor is to draw secondary flow for test cell cooling. The cooling flow requirement was set at 3000 SCFM as was stated in Chapter III. This requirement must be fulfilled while maintaining the compressor inlet pressure depression and engine back pressure values below the levels specified in the system design requirements. A one-dimensional, incompressible model, based on several simplifying assumptions and estimations, was developed to predict the performance parameters of the eductor. The incompressible assumption is based on the fact that exhaust flow Mach numbers were less than 0.3 over the entire range of calculations. As was stated in Chapter II, the design parameter that has the most effect on eductor performance is the eductor to primary nozzle area ratio. The model predicts the amount of secondary air flow drawn by the engine exhaust for varying exhaust nozzle sizes. It also predicts the pressure loss to the compressor and the engine back pressure for each nozzle size. Solutions are attained for nozzle diameters ranging from 8 inches to 6 inches which corresponds to eductor to primary nozzle area ratios from 12 to 23. The engine exhaust total pressure to cell pressure ratio ($P_o/P_{cell}$) throughout this range of eductor operation was estimated to be slightly greater than one. Results from Reference (4) indicate that a secondary to primary flow ratio in the range of one could be expected based on these conditions.

As shown in Figure (12), the two engine exhaust nozzles are centered in the 36 inch by 36 inch exhaust duct. The simple solution assumes symmetry between the two exhaust flows and is thus based on one eductor nozzle discharging into a 36 inch by 18 inch rectangular duct. The analysis was performed at 100 percent compressor speed and 100 percent design horsepower which corresponds to engine exhaust from each nozzle of 1.575 lbm/sec at 1061F.

A schematic representation of the simple eductor model is shown in Figure (13). Air at atmospheric conditions ($P_{atm}$= 14.696 psia, $T_{atm}$ =65F) is drawn into the cell by the engine compressor through the inlet ducting. The cell pressure, $P_{cell}$ is reduced below atmospheric pressure as a result of the pressure losses sustained in the inlet ducting. The engine exhaust (primary flow) at a mass flow rate of $w_p$ and velocity $V_1$ entrains air from the cell creating a secondary flow $w_s$ at velocity $V_2$ between the cell and point 2. Mixing of the primary and secondary flows occurs in the exhaust duct and is completed at an arbitrary point 3 in the exhaust ducting resulting in a total flow of $w_3$ at velocity $V_3$ . The fully mixed flow then exits the exhaust ducting at point e, 35 feet above the entrance to the inlet ducting.

The model assumes a steady primary flow with a uniform velocity profile at the nozzle exit and a steady, uniform, inviscid secondary flow from the cell to the exhaust duct entrance. Mixing in the exhaust duct is assumed to be adiabatic. The following parameters are assumed to be constant:

$w_1 = 1.575$ lbm/sec

$T_1 = 1061F$

$\rho_1 = 0.0261$ lbm/ft$^3$

$C_{p,1} = 204.61$ ft-lb/lbmR

$P_{atm} = 14.696$ psia

$T_2 = 65F$

$\rho_2 = \rho_{atm} = .0756$ lbm/ft$^3$

$C_{p,2} = 186.72$ ft-lb/lbmR

$A_3 = 4.5$ ft$^2$

$h = 35$ ft

The algorithm first applies conservation of mass, momentum, and energy equations across the eductor, the equation of state, and Bernoulli's equation to the secondary flow between the cell and the entrance to the eductor in order to solve for the secondary velocity ($V_2$), the secondary mass flowrate ($w_s$), and the total mass flowrate ($w_3$). Solution for these quantities in the eductor requires known values of $P_{cell}$ and $P_3$ which are applied on the front and back faces of the eductor respectively. Because $P_{cell}$ and $P_3$ are dependent on the pressure losses sustained in the inlet and exhaust ducts respectively, they are both functions of the total mass flow ($w_3$ ). Therefore an iterative technique is required. This technique involves attaining an initial solution for the total mass flow produced by the eductor with estimated values of $P_{cell}$, $P_3$, and $\rho_3$, and then using this initial solution to calculate new values of $P_{cell}$ , $P_3$, and $\rho_3$ to obtain an updated value for the total mass flow produced by the eductor. The itereration continues until convergence is achieved. This method of solution is repeated as the exhaust nozzle diameter is decreased from 8 inches in increments of 0.1 inches.

Estimates for $P_{cell}$ and $P_3$ are attained using applied fluid dynamics handbooks, References (1) and (2). These handbooks provide estimates for pressure loss coefficients in duct flow based on empirically derived equations and tables. Estimates for $P_{cell}$ and $P_3$ were determined using equations (2) and (3), with $\xi$ being the pressure loss coefficient associated with identified inlet and exhaust ducting loss sources. Equation (3) assumes adiabatic flow from point 3 to the exhaust duct exit point e.

$$P_{cell} = P_{atm} - \sum \frac{\xi_i \rho_i V_i^2}{2g_c} \tag{2}$$

$$P_3 = P_e + \frac{\rho_3 V_e^2}{2g_c} + \frac{\rho_3 g h}{g_c} - \frac{\rho_3 V_3^2}{2g_c} - \sum \frac{\xi_i \rho_3 V_i^2}{2g_c} \tag{3}$$

Where:

$$P_e = P_{atm} - \rho_{atm} \frac{g}{g_c} h$$

(3a)

The pressure loss coefficients (ξ) are a function of the geometry of each loss source and the Reynolds number of the flow at each loss source. This required that determination of the loss coefficients be based on an estimated total mass flow through the inlet and exhaust ducts. Results from reference (4) indicate that for the prescribed conditions in this problem, a total engine pressure to cell pressure ($P_o/P_{cell}$) of slightly greater than unity and an eductor to primary nozzle area ($A_3/A_1$) in the range of 12 to 23, a secondary to primary flow ratio ($w_s/w_p$) in the range of 1 could be expected. Determination of the pressure loss coefficients was therefore based on a total mass flow rate of twice the primary mass flowrate. Inlet ducting pressure loss sources and the corresponding pressure loss coefficients are shown in Table (1). Exhaust ducting loss sources and the corresponding pressure loss coefficients are shown below in Table (2). Note that in the calculation of the exhaust ducting loss coefficients, the exhaust temperature was assumed to be the average of the ambient temperature (65F) and the engine exhaust temperature (1061F).

## B. EDUCTOR ANALYSIS

Referring once again to Figure (13) the eductor analysis begins by assuming a constant primary mass flow for a prescribed exhaust nozzle diameter and solving for $V_1$:

$$V_1 = \frac{w_1}{\rho_1 A_1}$$

(4)

Assuming isentropic flow and a constant static pressure across the entrance plane of the eductor ($P_1=P_2$), and applying Bernoulli's equation between the cell and point 2:

$$P_{cell} = P_1 + \frac{\rho_2 V_2^2}{2g_c}$$

(5)

Applying the continuity and momentum energy equations between the inlet of the exhaust ducting and point 3:

$$\rho_1 A_1 V_1 + \rho_2 A_2 V_2 = \rho_3 A_3 V_3$$

(6)

$$P_1 A_1 + \frac{\rho_1 A_1 V_1^2}{2g_c} + P_2 A_2 + \frac{\rho_2 A_2 V_2^2}{2g_c} = P_3 A_3 + \frac{\rho_3 A_3 V_3^2}{2g_c}$$

(7)

25

Equations (4), (5),(6), and (7) are then combined in quadratic form to solve for $V_2$ in Equation (8):

$$V_2 = \frac{-b \pm \sqrt{b^2 - 4ac}}{2a}$$

(8)

where:

$$a = \frac{\rho_2^2 A_2^2}{\rho_3 A_3 g_c} + \frac{\rho_2 A_3}{2g_c} - \frac{\rho_2 A_2}{g_c}$$

(8a)

$$b = \frac{2\rho_1 A_1 V_1 \rho_2 A_2}{\rho_3 A_3 g_c}$$

(8b)

$$c = \left(P_3 - P_{cell}\right)A_3 + \frac{\left(\rho_1 A_1 V_1\right)^2}{\rho_3 A_3 g_c} - \frac{\rho_1 A_1 V_1^2}{g_c}$$

(8c)

The unknowns in equation (8) are the cell pressure $P_{cell}$, the eductor exit pressure $P_3$, and the eductor exit density $\rho_3$. Initial estimates of $P_3$ and $P_{cell}$ are made using equations (2) and (3) assuming only primary flow through both the inlet and exhaust ducts. The eductor exit density ($\rho_3$) is initially assumed to be the average of the engine exhaust density ($\rho_1$) and the cell density ($\rho_2$). These values are then substituted into equation (8) to obtain an initial estimate for the secondary velocity ($V_2$), from which estimated secondary and total mass flowrates are determined using equations (9) and (10).

$$w_2 = \rho_2 A_2 V_2$$

(9)

where:

$$A_2 = A_3 - A_1$$

(9a)

$$w_3 = w_1 + w_2$$

(10)

An updated value of $P_{cell}$ can then be determined using equation (2) based on the new estimate of the total mass flow rate. Before obtaining an updated value for $P_3$, the initial estimate of $\rho_3$ must be updated using the energy equation:

$$w_1 C_{p,1} T_{T1} + w_2 C_{p,2} T_{T3} = w_3 C_{p,3} T_{T3}$$

(11)

and the ideal gas equation:

26

$$P_3 = \rho_3 R T_3 \tag{12}$$

Approximating the total temperature as the static temperature with exhaust Mach numbers in the range of 0.1, equations (11) and (12) can be combined to solve for $\rho_3$:

$$\rho_3 = \frac{P_3}{(w_p C_{p,1} + w_s C_{p,2})(R \,/\, w_3 C_{p,3})} \tag{13}$$

The value for $P_3$ is then updated using equation (3), allowing calculation of an updated value for $V_2$ using equation (8). The iterations continue until convergence of $V_2$ is achieved resulting in a converged eductor solution for a given exhaust nozzle diameter. This procedure is then repeated as the nozzle diameter is decreased from 8 inches in increments of 0.1 inches.

The converged eductor solution can then be used to calculate the compressor inlet pressure ($P_c$) and the engine back pressure ($P_b$) for each nozzle diameter. Calculation of the compressor inlet pressure requires the use of references (1) and (2) to determine inlet plenum pressure loss coefficients ($\xi$). Determination of these loss coefficients is based on a mass flow rate equal to the total engine mass flow (3.15 lbm/sec) at ambient temperature (65F). The inlet plenum loss sources and their corresponding pressure loss coefficients are shown in Table (3). The compressor inlet pressure can then be calculated using equation (14) with $V_p$ equal to the velocity at the plenum inlet and $V_c$ equal to the velocity at the compressor inlet.

$$P_c = P_{cell} + \frac{\rho_{amb} V_p^2 g}{2 g_c} - \frac{\rho_{amb} V_c^2 g}{2 g_c} - \sum \frac{\rho_{amb} \xi_i V_i^2 g}{2 g_c} \tag{14}$$

Calculation of the engine back pressure requires calculation of the exhaust nozzle exit pressure ($P_1$) from equation (5), and determination of the engine exhaust piping pressure loss coefficients using references (1) and (2). The engine exhaust piping loss sources and their corresponding loss coefficients are shown in Table (4). Determination of the loss coefficients is based on a mass flow of 1.575 lbm/sec ($w_p$) at 1061F ($T_1$). The engine back pressure can then be calculated using equation (15) with $V_o$ equal to the velocity of the exhaust at the engine exhaust port.

$$P_b = P_1 + \frac{\rho_1 V_1^2 g}{2 g_c} - \frac{\rho_1 V_o^2 g}{2 g_c} - \sum \frac{\xi_i \rho_1 V_i^2 g}{2 g_c} \tag{15}$$

27

The MATLAB code written to perform the above analysis is included in the Appendix. The code essentially consists of three sections. The first section defines the initial conditions and constants. The second section consists of two iterative loops, an outer loop and an inner loop. The outer loop sets the exhaust nozzle diameter and area form which the exhaust nozzle velocity ($V_1$) is calculated. The initial estimate for the secondary velocity ($V_2$) is then calculated based on the initial estimates of $P_{cell}$, $P_3$, and $\rho_3$.

The inner loop then updates the values of $P_{cell}$, $P_3$, and $\rho_3$, and updates the value of $V_2$. The inner loop continues this iteration until convergence of $V_2$. This is the converged eductor solution for a particular nozzle size. The third section of the code then uses the converged eductor solution to calculate other parameters including compressor inlet pressure engine back pressure. Upon completion of these calculations the outer loop then reduces the exhaust nozzle diameter and the process is repeated.

## C. RESULTS

Results of the one-dimensional, incompressible analysis are shown in Figures (14) through (18). Figure (14) shows the exhaust nozzle velocity increasing from 175 ft/sec to 303 ft/sec as the nozzle diameter is decreased from 8 inches to 6 inches. The corresponding exhaust nozzle Mach number increases from 0.093 to 0.161 over this range of nozzle diameters.

Figure (15) shows the secondary to primary mass flow ratio increasing with decreasing exhaust nozzle diameter, ranging from about 1.3 for an 8-inch diameter nozzle to about 1.6 for a 6-inch diameter nozzle. This equates to a secondary flow ranging from approximately 3200 SCFM to 3900 SCFM which exceeds the secondary flow design requirement of 3000 SCFM. The increasing secondary to primary flow ratio with eductor to primary nozzle area ratio is consistent with results from References (4) and (5). The range of secondary to primary flow values obtained by the one-dimensional solution are slightly higher than the values obtained in Reference (4).

Figure (16) shows the cell pressure depression increasing with decreasing nozzle diameter and increasing nozzle velocity. The increasing nozzle velocities entrain more secondary flow which results in an increase in the total mass flow and greater pressure losses sustained in the inlet ducting. These results reflect this increase in inlet ducting pressure losses.

The amount of pressure depression at the compressor inlet from atmospheric inlet conditions is shown in Figure (17). The amount of depression at the compressor inlet predicted by the model ranges between a minimum of 1.28 in $H_2O$ to a maximum of 1.38 in $H_2O$. These values are well below the engine manufacturer quoted maximum value of compressor inlet depression (6 in $H_2O$) that could be sustained

without significantly effecting engine performance. Figure (18) shows the relationship between engine back pressure and exhaust nozzle exhaust velocity. The engine back pressure is computed as the difference between the inlet atmospheric pressure and the static pressure at the engine exhaust ports. These results indicate that a engine positive back pressure is not reached until a nozzle mach number of about 0.134 is reached. This corresponds to a nozzle velocity of about 252 ft/sec and a nozzle diameter of about 6.6 inches.
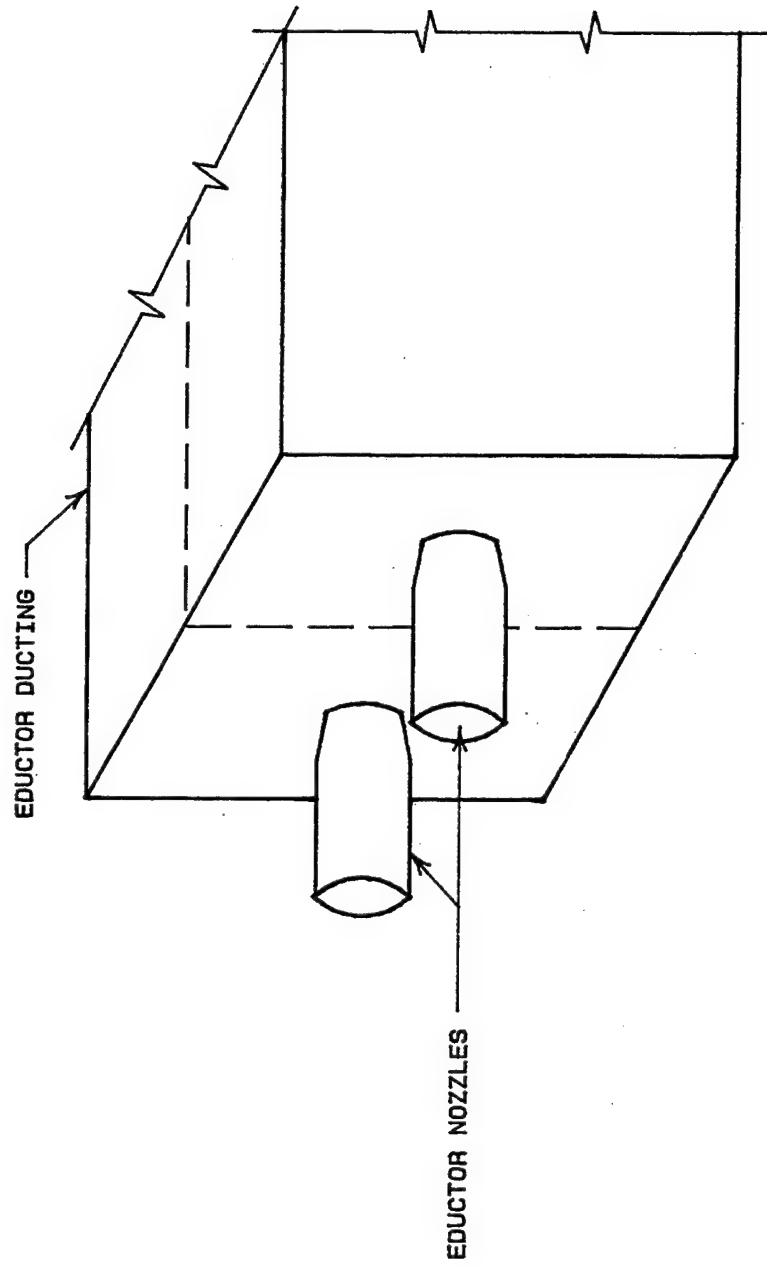
EDUCTOR DUCTING

EDUCTOR NOZZLES

Figure 12. Symmetry Assumption for One-Dimensional, Incompressible Solution.
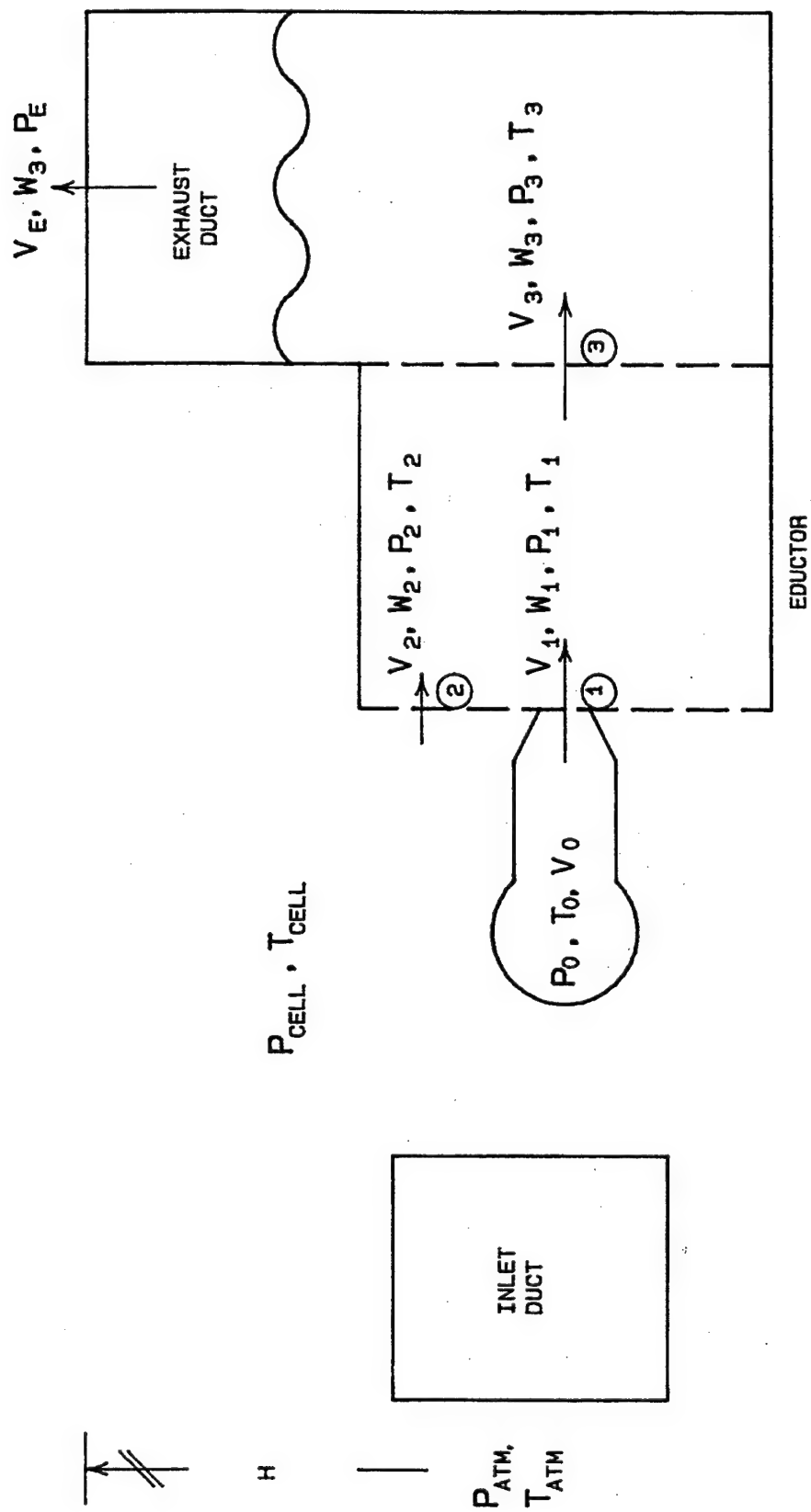
Figure 13. One-Dimensional, Incompressible Solution Schematic.

31

| Loss Source | Velocity (ft/sec) | Reynolds no. | Loss Coefficient, $\xi$ |
|---|---|---|---|
| 1. inlet louvers | 4.695 | 116,817 | 1.56 |
| 2. inlet screen | 4.695 | 116,817 | 0.5 |
| 3. silencers | 4.695 | 116,817 | 5.47 |
| 4. rectangular duct | 4.695 | 116,817 | 0.035 |
| 5. 90 degree bend | 4.695 | 116,817 | 1.14 |
| 6. inlet filter | 5.210 | 130,250 | * |
| 7. shutters | 5.210 | 130,250 | 1.5 |
| 8. duct exit | 5.210 | 130,250 | 2.0 |
| (n1= 100 %, w = 6.30 lbm/sec, T=65F, $\rho$ = .0756 lbm/ft$^3$, $\upsilon$ =1.6 $\times$ 10$^{-4}$ ft$^2$/sec) | | | |
| * inlet filter pressure loss data supplied by manufacturer | | | |

Table 1. Inlet Ducting Pressure Loss Coefficients

| Loss Source | Velocity (ft/sec) | Reynolds no. | Loss Coefficient, $\xi$ |
|---|---|---|---|
| 1. duct inlet | 18.0 | 110,204 | 0.50 |
| 2. 90 degree bend | 18.0 | 110,204 | 1.15 |
| 3. square duct | 18.0 | 110,204 | 0.018 |
| 4. transition to circular | 22.92 | 140,327 | 0.138 |
| 5. 90 degree bend | 22.92 | 140,327 | 0.40 |
| 6. circular duct | 22.92 | 140,327 | 0.21 |
| 7. exhaust to atmosphere | 22.92 | 140,327 | 1.2 |
| (n1=100 %, w = 6.30 lbm/sec, T=563F, $\rho$ = .0389 lbm/ft$^3$, $\upsilon$ = 4.90 $\times$ 10$^{-4}$ ft$^2$/sec) | | | |

Table 2. Exhaust Ducting Pressure Loss Coefficients

| Loss Source | Velocity (ft/sec) | Reynolds no. | Loss Coefficient,$\xi$ |
|---|---|---|---|
| 1. Inlet to flow meters | 47.16 | 221,063 | 0.32 |
| 2. Expansion into plenum | 59.69 | 248,708 | 0.91 |
| 3. Perforated plate (1 in) | 4.63 | 86,813 | 1.7 |
| 4. Perforated plate (1/2 in) | 4.63 | 86,813 | 2.4 |
| 5. 18-mesh screen | 4.63 | 86,813 | 1.2 |
| 6. 20-mesh screen | 4.63 | 86,813 | 2.8 |
| 7. Honeycomb screen | 4.63 | 86,813 | 2.0 |
| 8. Plenum contraction | 41.67 | 260,438 | 0.05 |
| 9. Compressor bellmouth | 94.32 | 442,125 | 0.3 |
| (n1=100%, w=3.15 lbm/sec, T=65F, $\rho$ = .0756 lbm/ft$^3$, $\upsilon$ =1.01$\times$ 10$^{-3}$ ft$^2$/sec) | | | |

Table 3. Inlet Plenum Pressure Loss Coefficients

| Loss source | Velocity (ft/sec) | Reynolds no. | Loss coefficient,$\xi$ |
|---|---|---|---|
| 1. Transition piece | 316.30 | 156,586 | 0.12 |
| 2. 90 degree elbow | 172.98 | 114,177 | 0.30 |
| 3. 73 degree bend | 172.98 | 114,177 | 0.243 |
| 4. Exhaust pipe | 172.98 | 114,177 | 0.256 |
| 5. 6 in nozzle | 307.5 | 152,228 | 0.045 |
| (n1=100%, w=1.575 lbm/sec, T=1061F, $\rho$ = .0261 lbm/ft$^3$, $\upsilon$ =1.01$\times$ 10$^{-3}$ ft$^2$/sec) | | | |

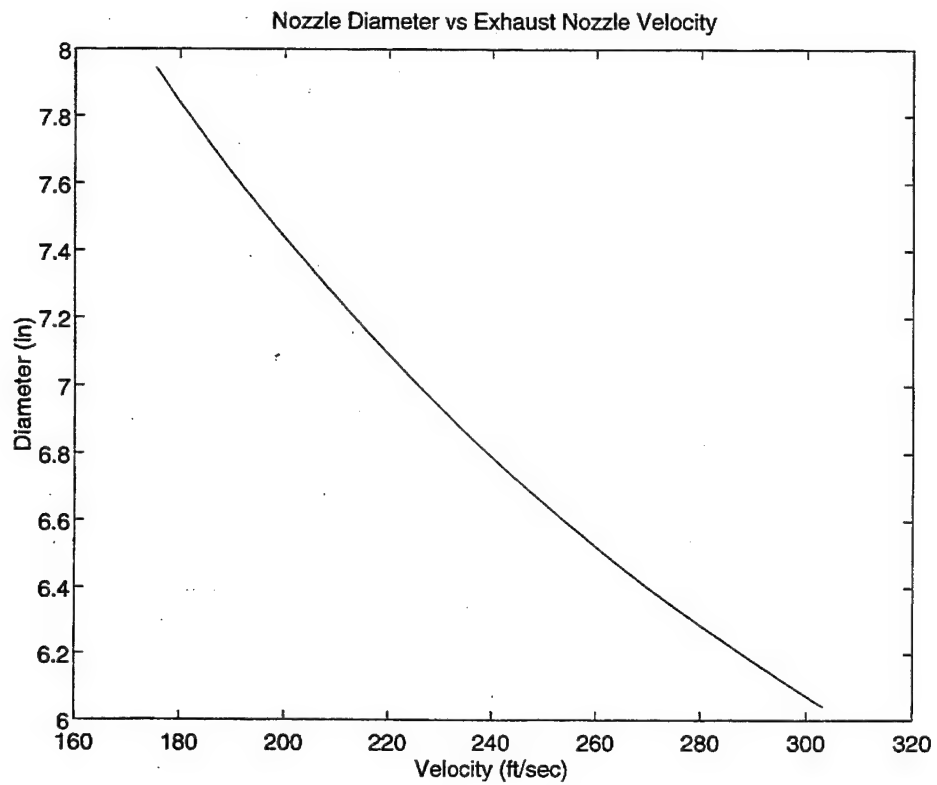Table 4. Exhaust Piping Pressure Loss Coefficients

Figure 14. Exhaust Nozzle Velocity vs. Nozzle Diameter, (1D Solution).



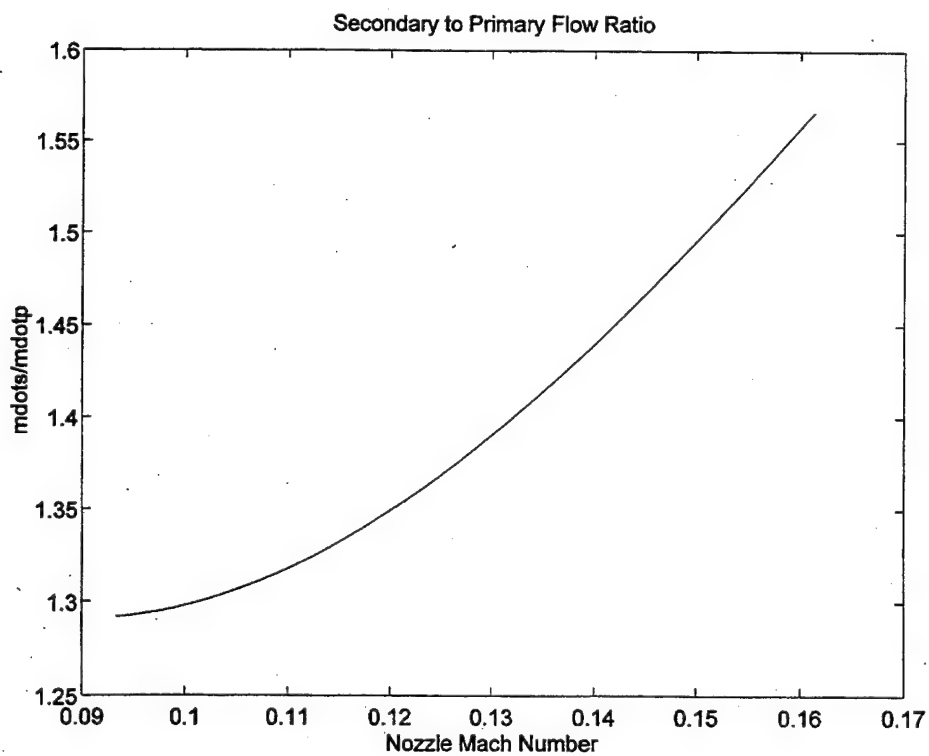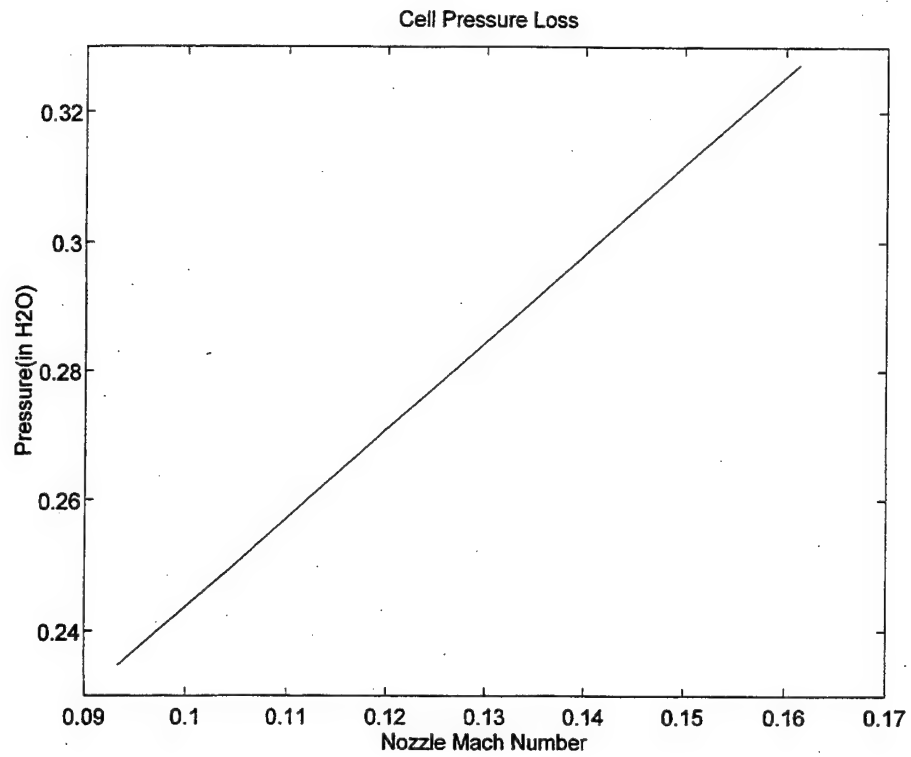Figure 15. Secondary to Primary Mass Flow Ratio, (1D Solution).

33

Cell Pressure Loss

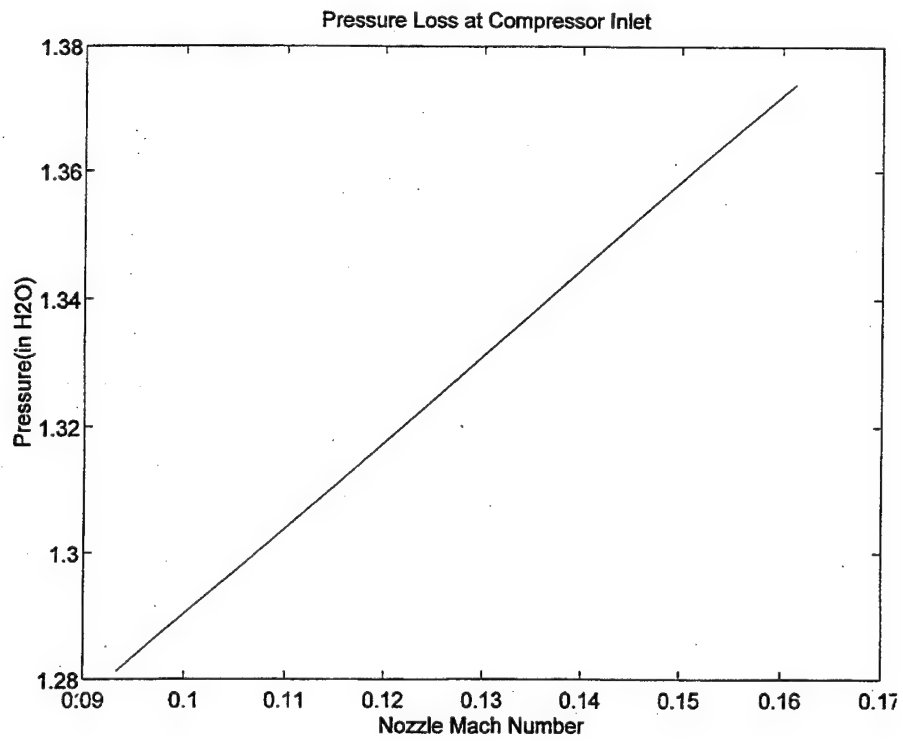Figure 16. Cell Pressure Loss, (1D Solution).

Pressure Loss at Compressor Inlet
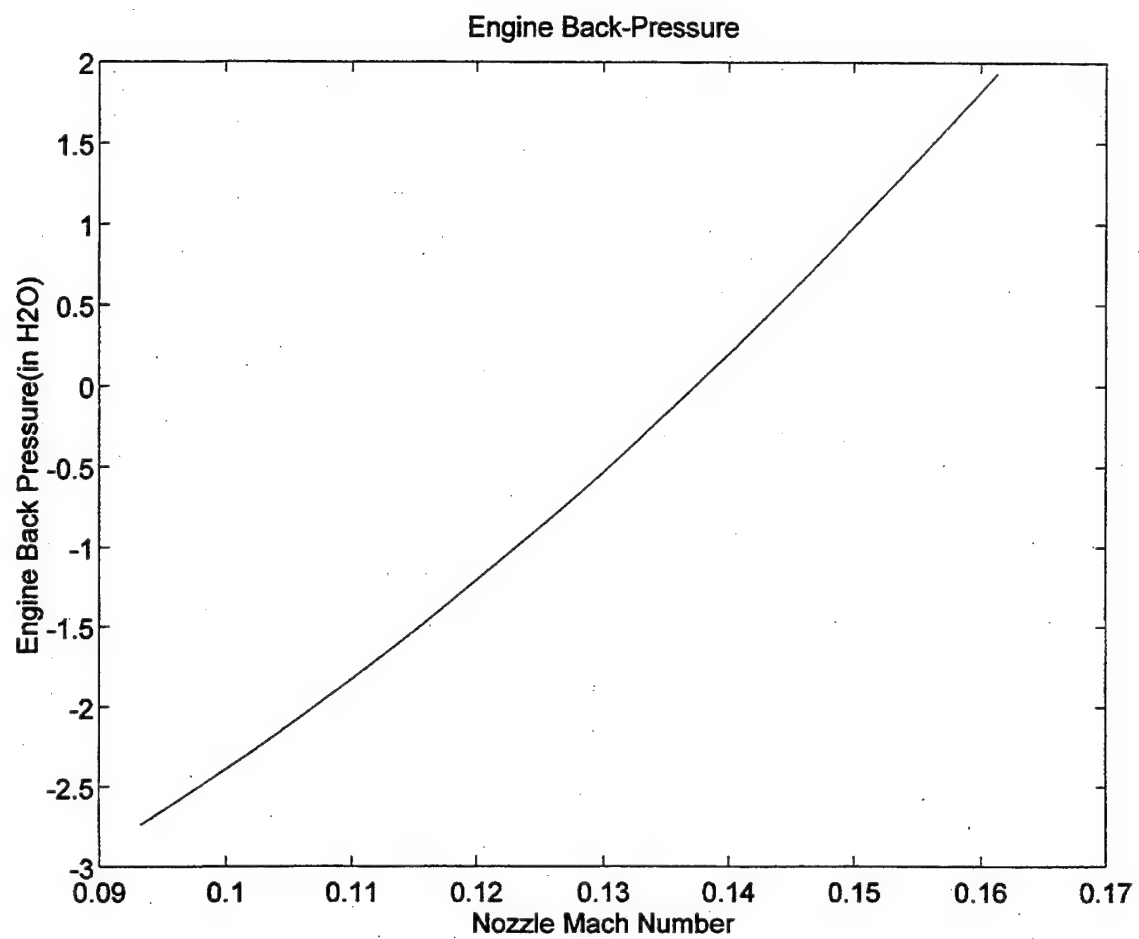
Figure 17. Compressor Inlet Pressure Loss, (1D Solution).

Figure 18. Engine Back-Pressure, (1-D Solution).

# V. COMPUTATIONAL FLUID DYNAMICS EDUCTOR MODEL

## A. PRELIMINARY CFD MODEL

A preliminary Computational Fluid Dynamics (CFD) model was developed to provide a more detailed analysis of the flow in the eductor. The specific goal of this preliminary analysis was to predict the velocity and temperature profiles developed in the entrance section of the exhaust ducting for prescribed primary and secondary flows. These results provide insight into the degree of mixing achieved in the entrance section of the exhaust ducting and a more precise picture of the flow.

This chapter describes the CFD model which essentially consists of a physical grid that simulates the exhaust eductor geometry and a CFD code which solves the appropriate state equations at each point in the eductor flow field. The velocity profiles and temperature contours generated by the CFD model are presented and described. The velocity profiles obtained from the CFD model are then compared against experimental results obtained on an eductor of similar geometry in order to verify the validity of the model.

## B. PHYSICAL GRID

The physical grid used is shown in Figure (19). The grid has a rectangular cross section and is 18 nozzle diameters in length. The outer walls of the grid correspond to walls of the exhaust duct. The symmetry assumption between the two exhaust nozzle flows is employed as it was with the one-dimensional model. An O-type (cylindrical) grid is used to allow simulation of the nozzle inlet flow at the front face of the grid. As can be seen on the front face, spacing in the radial direction is decreased at the outer edge of the nozzle and at the outer wall of the grid. This allows more precise calculation of flow in the nozzle shear layer and the wall boundary layer.

## C. FLOW SOLVER

OVERFLOW version 1.6ag, a FORTRAN CFD code developed at NASA Ames Research Center, was the flow-solver employed in the CFD model. The code first transforms grid points from the physical domain into the three-dimensional, Cartesian (rectangular) coordinate computational domain. The code then uses the ARC3D algorithm, which is an implicit, approximate factorization, finite differencing scheme to solve the Reynold's averaged Navier-Stokes Equations at each point in the computational domain. Viscous effects are simulated with the use of turbulence models. The code obtains solutions, i.e. density,

temperature, pressure, velocity, for the flow at each point in the computational domain, and then transforms these solutions back to the grid coordinates of the physical domain.

OVERFLOW was developed primarily to predict the flow over aerodynamic bodies and thus it initiates the flow-field with a specified free-stream value. Computations are performed and solutions are generated in the form of Q-vectors which are normalized by free-stream parameters. The normalized Q-vectors are computed as:

$$\overline{Q} = \begin{bmatrix} \rho^* \\ \rho^* u^* \\ \rho^* v^* \\ \rho^* w^* \\ e^* \end{bmatrix} \tag{16}$$

where:

$$\rho^* = \frac{\rho}{\rho_{inf}}, \qquad u^* = \frac{u}{a_{inf}}, \qquad v^* = \frac{v}{a_{inf}}, \qquad w^* = \frac{w}{a_{inf}}, \qquad e^* = \frac{e}{\rho_{inf} a_{inf}^2} \tag{16a}$$

with:

$\rho$ = density of the flow

$\rho_{inf}$ = density of the free stream

u = velocity in computational domain x direction

v = velocity in computational domain y direction

w = velocity in computational domain z direction

$a_{inf}$ = speed of sound at free stream conditions

The quantity e is the total energy defined by:

$$e = \rho C_v T_T + \frac{1}{2}\rho(u^2 + v^2 + w^2) \tag{16}$$

where:

$C_v$ = constant volume specific heat of the flow

$T_T$ = Total temperature of the flow

The pressure P can be related to the total energy by:

$$P = (\gamma - 1)\left(e - \frac{1}{2}\rho(u^2 + v^2 + w^2)\right) \tag{17}$$

where:

$\gamma$ = ratio of flow specific heats

38

## D. OVERFLOW INPUT FILE

The input file used in the CFD model is shown in Figure (20). Global parameters are entered in the first block including the number of iterations, NSTEP, which is set at 2000 iterations. Free-stream values are entered in the FLOINP block. Values for the secondary flow calculated from the one-dimensional solution for a 7-inch nozzle were entered as the free-stream values.

Selection and application of the turbulence model is done in the VISINP block. As can be seen in the first line in this block, the parameters VISCI, VISCJ, and VISCK were all set to "true" which has the effect of including viscous terms in all three computational directions. The Baldwin-Lomax turbulence model (see Reference (8)) was selected by setting ITTYPE to 1. This turbulence model is often employed in highly turbulent flows and was selected based on recommendations from the OVERFLOW User's Manual (Reference (8)). The remaining lines indicate the domain over which the turbulence model was employed. The turbulence model was employed over the entire domain due to the turbulent nature of the eductor flow.

Boundary conditions are prescribed in the BCINP block. A total of 6 boundary conditions were prescribed. Each column in this block represents the description of one boundary condition. The IBTYP line indicates the type of boundary condition and the remaining lines indicate the region over which the boundary conditions are employed. The first column (IBTYP 42) in this block describes the nozzle inflow boundary condition. This is a prescribed boundary condition which must be read in from a separate file. The prescribed boundary condition file is shown in Figure (21). The normalized Q-vectors corresponding to the exhaust nozzle inflow were applied to the nozzle inflow portion on the front face of the physical grid (Figure (19)).

The second column of the BCINP block of Figure (20) describes the remainder of the front face of the physical grid minus the nozzle inflow face. IBTYP 40 identifies this portion of the grid as an inflow surface and assigns the free-stream values to this surface. The fourth column describes the outer walls of the physical grid. IBTYP 5 identifies this portion of the physical grid as a viscous adiabatic wall. The fifth column (IBTYP 5) identifies the back face of the physical grid as an outflow surface. The remaining boundary conditions, IBTYP 10 and IBTYP 14, are related to the type of physical grid (O-type) chosen.

## E. RESULTS

The velocity profiles attained from the converged solution of the CFD model in the mid-plane cross section of the physical grid are shown in Figure (22). The central portion of the initial velocity profile on the bottom plane of the grid represents the high velocity primary flow from the engine nozzle. The outer

39

portions of this profile represent the free-stream or secondary flow. The high-velocity exhaust nozzle entrains the free-stream secondary flow and a profile with increased mixing width and reduced centerline velocity emerges at approximately seven to eight nozzle diameters into the exhaust duct. From this point further spread of the jet core is minimal as the velocity profile remains basically constant through the end of the duct. The reduction in centerline velocity from the duct entrance to the eighth nozzle diameter is approximately 33 percent.

The temperature contour from the converged solution is shown in Figure (23). The bottom shows the entry of the high temperature primary flow in red along with the lower temperature secondary flow in black. Mixing of the two flows occurs throughout the length of the duct resulting in a much more uniform temperature profile at the duct exit.

The velocity profiles obtained from the CFD model were compared against velocity profiles obtained experimentally on an eductor of similar geometry. The experimental results taken from Reference (2), were for ambient temperature flow through a cylindrical eductor with a mixing tube to exhaust nozzle area ratio of approximately 13. The CFD results were obtained for a mixing tube to exhaust nozzle area ratio of approximately 16 and a primary flow to secondary flow temperature ratio of approximately 2.6 at the eductor inlet. Reference (9) cites experimental and analytical results obtained for the mixing coaxial turbulent jets in a pipe with different temperatures and velocitys. These results indicated that the degree of influence that the temperature ratio had on the mixing of the two jets was insignificant. The range of temperature ratios tested in these experiments was between 1.1 and 1.2.

Results of the comparison are shown in Figure (24). The velocity profiles are plotted at three points downstream of the mixing tube entrance. The downstream length x is normalized by the mixing tube diameter D. At 1.8 mixing tube diameters the experimental and CFD profiles are similar in that both show about a 5 percent decay in the centerline jet velocity. A slightly greater degree of mixing has been achieved in the CFD profile as indicated by the greater degree of spread. At 3.4 mixing tube diameters there is less agreement between the two profiles. The reduction in centerline velocity of the CFD profile is about 28 percent compared to about 45 percent in the experimentally obtained profile. The experimenttally obtained profile also shows that a slightly greater degree of mixing has been achieved. A big disparity between profiles is indicated at 5.8 mixing tube diameters. The experimentally obtained profile shows a 72 percent reduction of jet centerline velocity compared to about 33 percent for the CFD profile. The experimentally obtained profile is also much more uniform than the CFD profile which indicates a much greater degree of mixing has been achieved in the experimental profile.
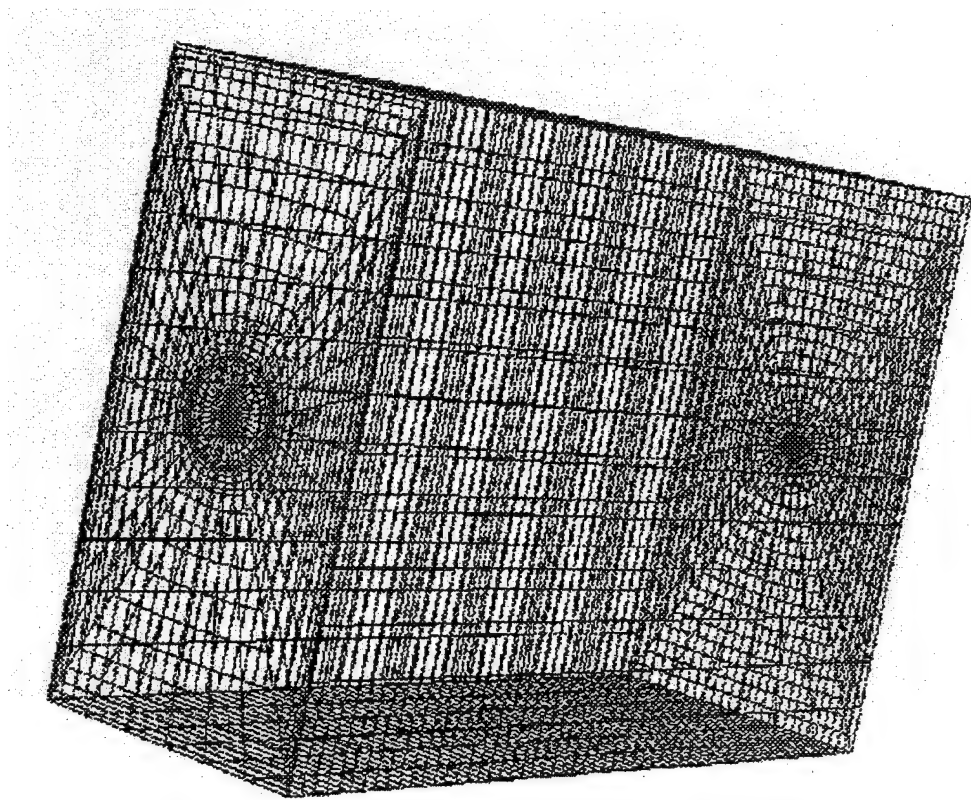
Figure 19. CFD Physical Grid.

```
$GLOBAL
     CHIMRA= .F.,   NSTEPS= 2000,   RESTRT= .F.,   NSAVE = 50,
     NQT    = 0,
     $END
$FLOINP
     ALPHA = 0.0,   FSMACH= 0.00651,   REY   = 0.82294E5,   TINF  = 525.0,
     $END
$VARGAM $END




$GRDNAM
     NAME = 'NACA 0012 Baldwin-Barth Grid (Alpha 2.26/M .799/Re 9 mil)',
$END
$NITERS
     $END
$METPRM
     IRHS  = 0,   ILHS  = 2,   IDISS = 2,
     $END
$TIMACU
     ITIME = 1,   DT    = 1.0,
     $END
$SMOACU
     ISPECJ= 2,   DIS2J = 2.00,   DIS4J = 0.02,
     ISPECK= 2,   DIS2K = 2.00,   DIS4K = 0.02,
     ISPECL= 2,   DIS2L = 2.00,   DIS4L = 0.02,
     SMOO  = 1.00,
     $END
$VISINP
     VISCJ = .T.,   VISCK = .T.,   VISCL = .T.,
     NTURB  = 1,
     ITTYP  = 1,
     ITDIR  = -2,
     JTLS·  = 1,
     JTLE · = 37,
     KTLS   = 1,
     KTLE   = 16,
     LTLS   = 2,
     LTLE   = 57,
     TLPAR1= -1.,
     $END
$BCINP
     NBC   =   6,
     IBTYP =  42, 40, 10,  5,  32, 14,
     IBDIR =   3,  3,  1, -2,  -3,  2,
     JBCS  =   1,  1,  1,  1,   1,  1,
     JBCE  =  37, 37,  1, 37,  37, 37,
     KBCS  =   1,  8,  1, 16,   1,  1,
     KBCE  =   7, 16, 16, 16,  16,  1,
     LBCS  =   1,  1,  1,  2,  57,  1,
     LBCE  =   1,  1, 57, 57,  57, 57,
     BCFILE(1) = 'bc1.save',
     $END
$SCEINP $END
```

Figure 20. CFD Input File.

42

```
c-------------------------------------------------------------------------------c
c-------------------------------------------------------------------------------c
c       parameter (jn=37,kn=7,ln=57,qn=6)
        DIMENSION q(37,7,1,6)
        OPEN(unit=12,file='bc1.save',status='unknown',form='unformatted')
        OPEN(unit=14,file='bc1.for',status='unknown',form='formatted')
        jn=37
        kn=7
        ln=1
        qn=6
        fsmach=0.00651
        alpha=0
        Re=82294
        time=1
        gaminf=1.4
        q1=0.3421
        q2=0.0688
        q3=0.0
        q4=0.0
        q5=2.021
        q6=1.353
        print *,q1,q2,q3,q4,q5,q6
        do 10 j=1,jn
          do 10 k=1,kn
                q(j,k,ln,1)=q1
                q(j,k,ln,2)=q2
                q(j,k,ln,3)=q3
                q(j,k,ln,4)=q4
                q(j,k,ln,5)=q5
                q(j,k,ln,6)=q6
10      continue
        WRITE(12) jn,kn,ln
        WRITE(12) fsmach,alpha,Re,time,gaminf
        WRITE(12) ((((q(j,k,1,nq),j=1,jn),k=1,kn),l=1,ln),nq=1,qn)
        WRITE(14,*) jn,kn,ln
        WRITE(14,*) fsmach,alpha,time,gaminf
        WRITE(14,*) ((((q(j,k,1,nq),j=1,jn),k=1,kn),l=1,ln),nq=1,qn)
        close(12)
        close(14)
        STOP
        END
```

Figure 21. Prescibed Nozzle Flow Input File.

43

high velocity nozzle exhaust

entrained secondary flow
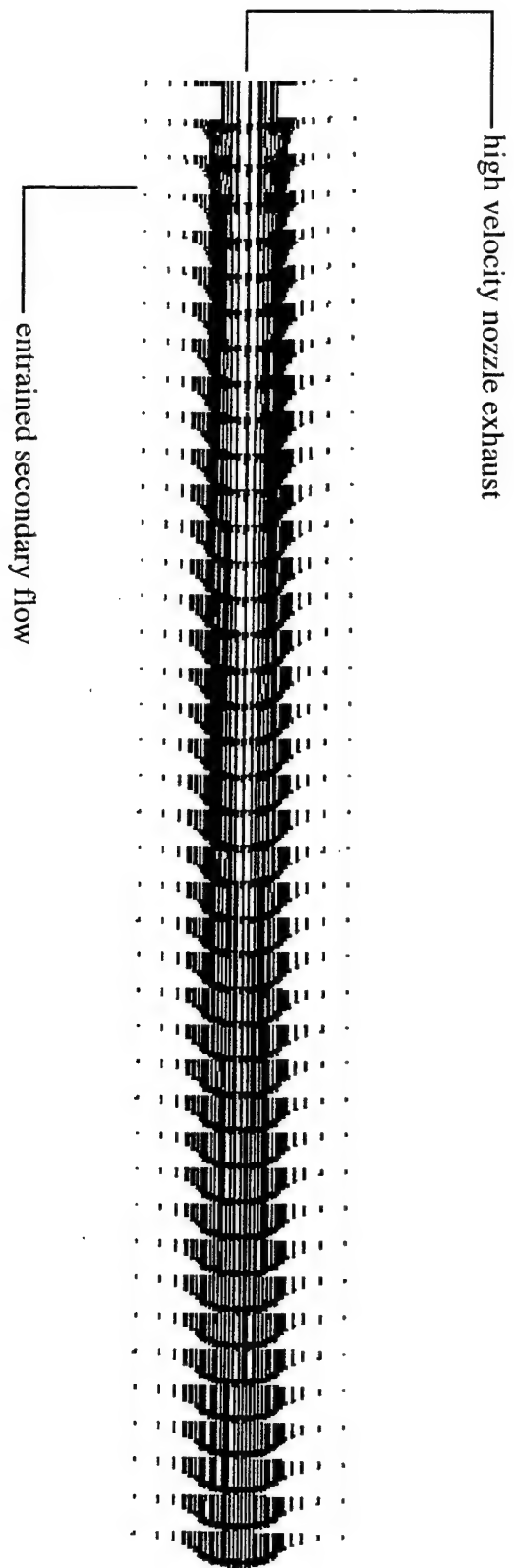
Figure 22. CFD Eductor Centerline Velocity Profiles.

44

low temperature entrained secondary flow

high temperature nozzle exhaust into eductor
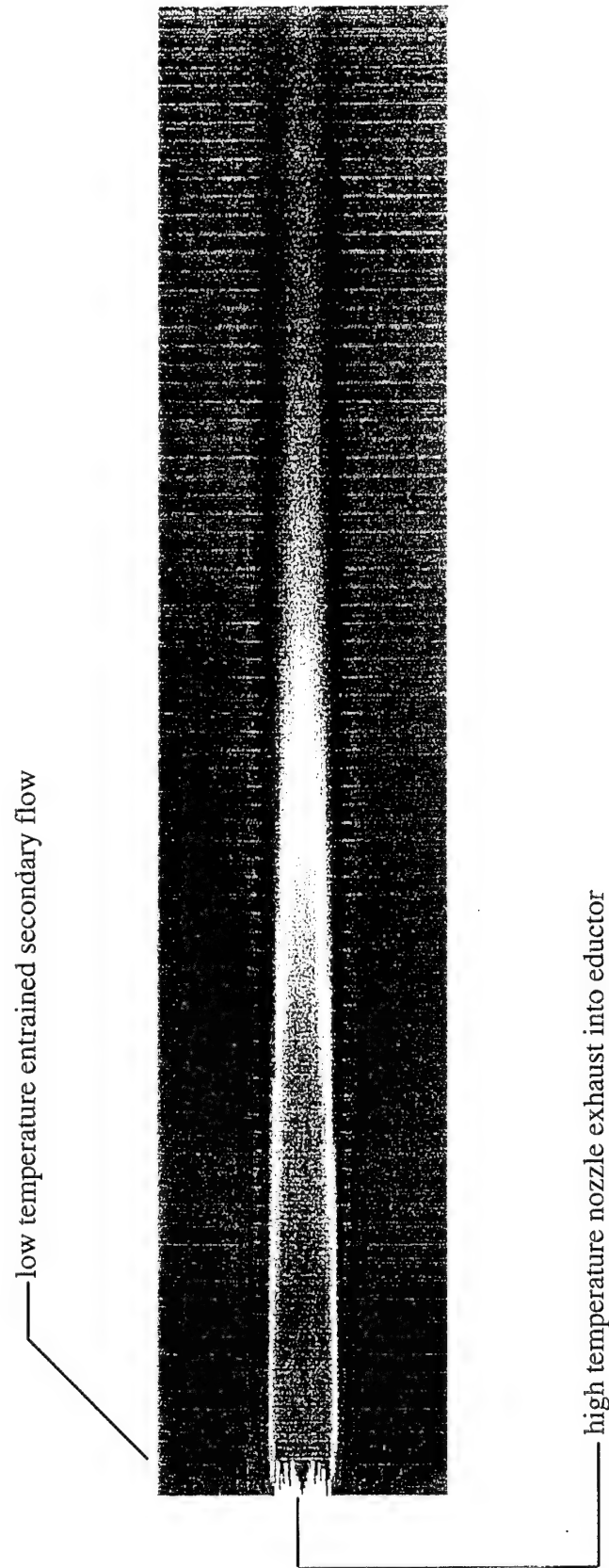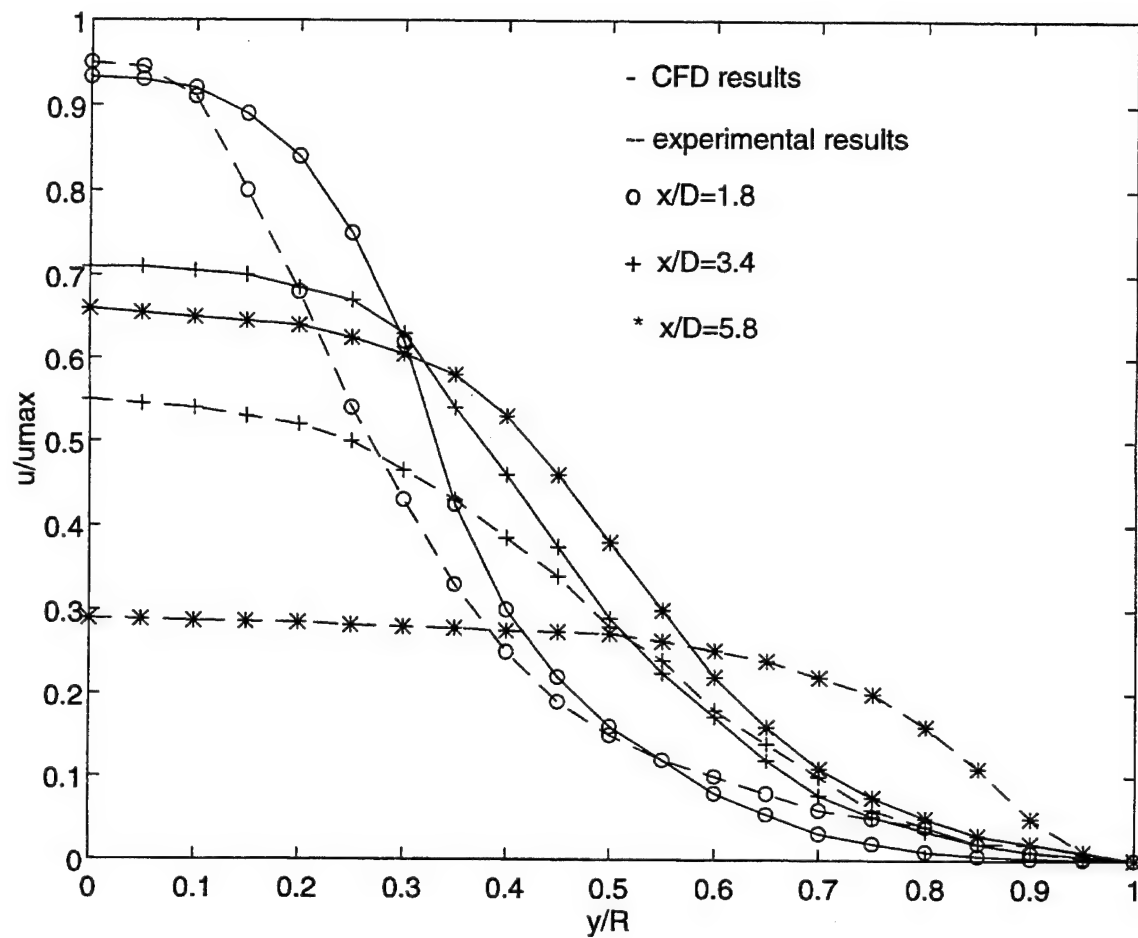
Figure 23. CFD Eductor Centerline Temperature Contours.

Figure 24. Comparison of CFD Velocity Profiles Against Experimental Results,
(experimental results from Ref (9)).

# VI. CONCLUSIONS AND RECOMMENDATIONS

## A. CONCLUSIONS

An air system has been designed that meets the system design objectives. Achievement of the system performance objectives was verified through analysis. Specifically, the air system should:

1. Provide clean and uniform flow to the engine compressor at the required full power rate of 2500 SCFM.
2. Provide the capabilty to observe, measure, and modify the the compressor inlet profile so that proper uniformity can be attained through iterative testing.
3. Provide the required secondary cell cooling flow requirement of 3000 SCFM at full power operation with an installed exhaust eductor.
4. Provide the required system performance measurement and engine noise attenuation capabilities.
5. Maintain compressor inlet depression well below the maximum level of 6 in $H_2O$.
6. Maintain engine back pressure below 2 in $H_2O$.

Two analytical models were developed which were used to evaluate eductor performance. A one-dimensional, incompressible eductor model was developed that predicts the amount of secondary airflow drawn for varying eductor nozzle sizes. The one-dimensional model also predicts overall air system parameters including cell pressure, compressor inlet pressure, engine back pressure, and eductor exhaust pressure and temperature. The model verifies that the eductor produces the required secondary airflow specified in the design objectives.

A preliminary eductor computational fluid dynamics model was developed to evaluate the flow in the eductor. A physical grid was created for a specified eductor configuration. Velocity profiles and temperature contours were produced for specified primary and secondary eductor flows. Comparison of the velocity profiles with profiles obtained experimentally on an eductor of similar geometry revealed that the profiles develop as expected to a point slightly greater than halfway into the mixing tube. Beyond this point minimal mixing is achieved and the velocity profiles do not develop as rapidly as would be expected based on comparison with the experimental results.

## B. RECOMMENDATIONS

The one-dimensional analytical model can be improved by formulating equations for the inlet and exhaust ducting pressure loss coefficients, which are dependent on the total mass flow, and integrating the equations into the iterative loop. The model can be also be expanded to provide analysis for other engine operating conditions.

The CFD model can be improved to provide expanded analysis of the eductor flow. Specifically:
1. The input file can be modified to allow prediction of axial secondary flow entrainment with imposed pressure conditions on the front and back faces of the physical grid.
2. The physical grid can be modified to allow prediction of axial and radial secondary flow entrainment as the spacing between the exhaust nozzle and the mixing tube entrance is varied.
3. The physical grid can also be expanded to model part or all of the exhaust ducting. Of particular interest would be analysis of the exhaust flow as it turns from the short vertical entrance section into the main horizontal section of exhaust ducting. This analysis could provide important insight into potential eductor design improvements.

The air system is designed so that the optimum eductor configuration can be verified through testing. Readings for the total mass flow should be taken as the exhaust nozzle diameter and exhaust nozzle to eductor inlet separation are varied. The total mass flow could be measured by taking a cross-sectional grid of velocity measurements as the flow exits the inlet ducting with a constant-temperature anemometer. Cell pressure, compressor inlet pressure, and engine back pressure can also be verified for varying eductor configurations. Testing should also be conducted to verify uniformity of the compressor inlet velocity profiles. Observation of the compressor inlet profile can be achieved with the use of a smoke wand in the inlet plenum. This profile can also be measured by taking a cross-sectional grid of velocity readings at the compressor inlet.

Any modification to the basic eductor design that increases the degree of mixing achieved in the initial vertical section of the exhaust ducting should improve the eductor performance. Enhanced mixing could potentially be achieved through the use of corrugated exhaust nozzles. These nozzles would introduce large scale axial vortex structures in the exhaust flow that should promote enhanced mixing. This offers another potential area for evaluation and testing.

48

## APPENDIX. MATLAB CODE FOR ONE-DIMENSIONAL, INCOMPRESSIBLE EDUCTOR MODEL

The matlab code shown below was written based on the simple, incompressible method of solution presented in Chapter 3.

```
% incompressible solution, varying nozzle area, rho3 from energy eqn,
% varying cell pressure, varying eductor outlet pressure, full power
clear
% define constants and initial estimates
gc=32.17;
r=53.34;
rho1=.0261;
rho2=.0756;
rho3g=.0389;
t1=1521;
t2=525;
gamma1=1.353;
c1=(gc*gamma1*r*t1)^.5;
mdotp=3.15/2;
a3=4.5;
patm=2116.2;
pcellg=patm;
pe=patm-(rho2*35);
p3g=patm;
cp1=204.61;
cp2=186.72;
cp3=193.72;
% initial calculation for v2, mdots, mdot3
for i=1:30;
% input primary nozzle area a1
a1(i)=.3491-(.005*i);
% nozzle diameter d
d(i)=2*((a1(i)*144/pi)^.5);
% secondary flow area a2
a2(i)=a3-a1(i);
% nozzle velocity v1
v1(i)=mdotp/(rho1*a1(i));
% nozzle mach no. m1
m1(i)=v1(i)/c1;
ag(i)=(((rho2*a2(i))^2)/(gc*rho3g*a3))+((rho2*a3)/(2*gc))-((rho2*a2(i))/gc);
bg(i)=(2*mdotp*rho2*a2(i))/(gc*rho3g*a3);
cg(i)=((p3g-pcellg)*a3)-((mdotp*v1(i))/gc)+((mdotp^2)/(gc*rho3g*a3));
eg(i)=(bg(i)^2-(4*ag(i)*cg(i)))^.5;
% initial solution for v2, mdotp, mdot3
v2g(i)=(-bg(i)+eg(i))/(2*ag(i));
mdotsg(i)=rho2*a2(i)*v2g(i);
mdot3g(i)=mdotp+mdotsg(i);
v2i(1)=v2g(i);
mdotsi(1)=mdotsg(i);
mdot3i(1)=mdot3g(i);
% inner loop iterate through convergence of v2
for j=1:100;
% calculate rho3 with energy equation
t3(j)=((mdotp*cp1*t1)+(mdotsi(j)*cp2*t2))/(mdot3i(j)*cp3);
```

```
rho3(j)=p3g/(r*t3(j));
% inlet ducting velocities
vin1(j)=mdot3i(j)/(rho2*17.75);
vin2(j)=mdot3i(j)/(rho2*16);
% calculate inlet ducting losses
plin(j)=0.6+((rho2/(2*gc))*((12.205*vin1(j)^2)+(3.5*vin2(j)^2)));
% calculate cell pressure
pcell(j)=(patm-plin(j));
% calculate exhaust ducting velocities
v31(j)=mdot3i(j)/(rho3(j)*9);
v32(j)=mdot3i(j)/(rho3(j)*7.069);
% exhaust ducting losses
plout(j)=(rho3(j)/(2*gc))*((1.668*v31(j)^2)+(1.948*v32(j)^2));
% eductor exit pressure (absolute)
p3(j)=pe+plout(j)+(rho3(j)*35)+((rho3(j)/(2*gc))*(v32(j)^2-v31(j)^2));
% update solution for v2, mdots, mdot3
a(j)=(((rho2*a2(i))^2)/(gc*rho3(j)*a3))+((rho2*a3)/(2*gc))-((rho2*a2(i))/gc);
b(j)=(2*mdotp*rho2*a2(i))/(gc*rho3(j)*a3);
c(j)=((p3(j)-pcell(j))*a3)-((mdotp*v1(i))/gc)+((mdotp^2)/(gc*rho3(j)*a3));
e(j)=(b(j)^2-(4*a(j)*c(j)))^.5;
v2i(j+1)=(-b(j)+e(j))/(2*a(j));
mdotsi(j+1)=rho2*a2(i)*v2i(j);
mdot3i(j+1)=mdotp+mdotsi(j+1);
del(j)=abs(v2i(j+1)-v2i(j));
if del(j)<=0.1, break, end
end
% converged values for v2, mdots, mdot3
v2(i)=v2i(j+1);
mdots(i)=v2(i)*rho2*a2(i);
mdot3(i)=mdots(i)+mdotp;
% cell pressure loss
pcellos(i)=plin(j)*(33.91*12/2116);
% nozzle exit pressure (absolute)
p1(i)=pcell(j)-((rho2*v2(i)^2)/(2*gc));
% engine total pressure (absolute)
po(i)=p1(i)+((rho1*v1(i)^2)/(2*gc));
% calculate exhaust piping velocities
vpin(i)=mdotp/(rho1*pi*3.5*2.5/144);
vpout(i)=mdotp/((rho1*pi*(d(i)/2)^2)/144);
vp(i)=mdotp/(rho1*.3491);
% exhaust piping pressure loss
pploss(i)=((.12*rho1*vpin(i)^2)/(2*gc))+((.844*rho1*vp(i)^2)/(2*gc));
% engine back pressure
pback1(i)=p1(i)+((rho1*vpout(i)^2)/(2*gc))-((rho1*vpin(i)^2)/(2*gc))+pploss(i);
pback(i)= (pback1(i)-2116.2)*(33.91*12/2116.2);
% calculate inlet plenum velocities;
vpl1(i)=(mdotp/rho2)/.442;
vpl2(i)=(mdotp/rho2)/9;
vpl3(i)=(mdotp/rho2);
vpl4(i)=(mdotp/rho2)/.267;
% inlet plenum pressure loss
plen(i)=((1.23*rho2*vpl1(i)^2)/(2*gc))+((9.6*rho2*vpl2(i)^2)/(2*gc))...
+((.05*rho2*vpl3(i)^2)/(2*gc))+((.3*rho2*vpl4(i)^2)/(2*gc));
% calculate pressure loss at compressor inlet
pcomp(i)=(plin(j)+plen(i))*(33.91*12/2116.2);
```

```
end
figure(1)
plot(v1,d)
title('Nozzle Diameter vs Exhaust Nozzle Velocity')
xlabel('Velocity (ft/sec)')
ylabel('Diameter (in)')
figure(2)
plot(m1,d)
title('Nozzle Diameter vs. Exhaust Nozzle Mach no.')
xlabel('Nozzle Mach Number')
ylabel('Nozzle Diameter(in)')
figure(3)
plot(m1,mdots/mdotp)
title('Secondary to Primary Flow Ratio')
xlabel('Nozzle Mach Number')
ylabel('mdots/mdotp')
figure(4)
plot(m1,po)
title('Engine Total Pressure')
xlabel('Nozzle Mach Number')
ylabel('Total Pressure (psf)')
figure(5)
plot(m1,pback)
title('Engine Back-Pressure')
xlabel('Nozzle Mach Number')
ylabel('Engine Back Pressure(in H2O)')
figure(6)
plot(m1,p1)
title('Nozzle Exit Pressure')
xlabel('Nozzle Mach Number')
ylabel('Nozzle Exit Pressure(psf)')
figure(7)
plot(m1,pcellos)
title('Cell Pressure Loss')
xlabel('Nozzle Mach Number')
ylabel('Pressure(in H2O)')
figure(8)
plot(m1,pcomp)
title('Pressure Loss at Compressor Inlet')
xlabel('Nozzle Mach Number')
ylabel('Pressure(in H2O)')
```

# LIST OF REFERENCES

1. Blevins, R. D., "*Applied Fluid Dynamics Handbook*", Krieger Publishing Co., 1992.

2. Idelchik, I. E., "*Handbook of Hydraulic Resistance*", Hemisphere Publishing Corporation,1986.

3. Abramovich, G. N., " *The Theory of Turbulent Jets*", The Massachusetts Institute of Technology, 1963.

4. Keenan, J. H., and Neumann, E. P., " *A Simple Air Ejector*", Journal of Applied Mechanics, June 1942.

5. Ellen., C. R., "*Model Tests of Multiple Nozzle Exhaust Gas Eductor Systems for Gas Turbine Powered Ships*", Thesis, Naval Postgraduate School, Monterey, Ca. June 1977.

6. Allison Gas Turbines "*Model-C18 Installation Design Manual*", 1976.

7. Pope, A., and Harper, J. J., "*Low Speed Wind Tunnel Testing*", John Wiley and Sons Inc., 1966.

8. Buning, P. G., Chan, W. M., Renze, K. J., Sondak, D. L., Chiu, I. T., and Slotnick, J. P., "*OVERFLOW User's Manual*", NASA Ames Research Center, April 1993.

9. Schlichting, H. "*Boundary Layer Theory*", seventh edition, McGraw-Hill Inc., 1987.

# INITIAL DISTRIBUTION LIST

|  | No. Copies |
|---|---|
| 1. Defense Technical Information Center<br>8725 John J. Kingman Rd., STE 0944<br>Ft. Belvoir, Virginia 22060-6218 | 2 |
| 2. Library, Code 13<br>Naval Postgraduate School<br>Monterey, California 93943-5101 | 2 |
| 3. Department Chairman, Code ME<br>Department of Mechanical Engineering<br>Naval Postgraduate School<br>Monterey, California  93942-5000 | 2 |
| 4. Professor Knox T. Millsaps, Jr., Code ME/Mi<br>Department of Mechanical Engineering<br>Naval Postgraduate School<br>Monterey, California 93942-5000 | 2 |
| 5. Curricular Officer, Code 34<br>Department of Mechanical Engineering<br>Naval Postgraduate School<br>Monterey, California 93942-5000 | 1 |
| 6. LT David D. Phelps<br>PREINSURV SEA DUTY DET<br>Norfolk, Virginia 23521 | 2 |